Universidade de Aveiro
2017
Departamento de Engenharia de Materiais e Cerâmica

Hugo Filipe Delgado Almeida

Biomembranas de poliuretano produzidas por electrofiação para enxertos vasculares

Electrospun polyurethane biomembranes for vascular grafts

Universidade de Aveiro
2017
Departamento de Engenharia de Materiais e Cerâmica

Hugo Filipe Delgado Almeida

Biomembranas de poliuretano produzidas por electrofiação para enxertos vasculares

Electrospun polyurethane biomembranes for vascular grafts

Tese apresentada à Universidade de Aveiro para cumprimento dos requisitos necessários à obtenção do grau de Mestre em Materiais e Dispositivos Biomédicos realizada sob a orientação científica da Doutora Maria Helena Figueira Vaz Fernandes, Professora associada e da Doutora Maria Elizabete Jorge Vieira Da Costa, Professora auxiliar do Departamento de Engenharia de Materiais e Cerâmica da Universidade de Aveiro

“The only time I set the bar low is for limbo.”

-Michael Scott

o júri

presidente

Prof. Doutor Francisco Manuel Lemos Amado
Professor Associado com Agregação no Departamento de Química da Universidade de Aveiro

Doutora Paula Alexandrina de Aguiar Pereira Marques
Equiparada a Investigadora Principal, Universidade de Aveiro

Prof. Doutora Maria Helena Figueira Vaz Fernandes
Professora associada no Departamento de Engenharia de Materiais e Cerâmica da Universidade de Aveiro. (Orientadora)

acknowledgements

Throughout this work I had the support of several people to whom I owe a sincere thank you.

Firstly, I would like to thank Professors Maria Helena Figueira Vaz Fernandes and Maria Elizabete Jorge Vieira da Costa for the opportunity, the support and the availability demonstrated from the start. To Professor Cláudia Oliveira for the aid provided regaring some aspects of the experimental work. To the entire technical team of the Department of Materials and Ceramics Engineering (DEMAC) for the immense support shown.

To Adriana Magueta, Ana João, André Girão, Andreia Pereira, Gonçalo Ramalho, Joana Baltazar and Nathalie Barroca, for all the good moments in the lab, the friendship and for all the knowledge bestowed upon me.

To Eduardo Seabra, João Martins, Pedro Luis and Tiago Marques for all the crazy adventures.

To those who supported me and believed in me, but are no longer here to witness my achievements.

And lastly to my parents, for the unconditional support, love and for all the sacrifices they made. What I have, and am I owe it to both of you.

palavras-chave Membranas compósitas, Poliuretano, Oxido de Zinco, Propiedades antibacterianas, Propriedades mecânicas, Enxertos vasculares.

resumo

Um dos grandes desafios da engenharia de tecidos (TE) vasculares, prende-se com a pouca disponibilidade de tecidos vasculares autólogos para substituição de vasos sanguíneos de pequeno diâmetro (<6 mm). Estudos demonstram que o poliuretano possui propriedades mecânicas adequadas para a utilização em vasos sanguíneos de pequenos diâmetros. Trabalhos anteriores realçam as propriedades antibacterianas de compósitos compostos por PU e nanopartículas de oxido de zinco (nZnO).

O presente estudo teve como objetivo a produção de membranas compósitas de PU/ nZnO com recurso a electrofiação. Mais concretamente pretendia-se avaliar as propriedades antibacterianas e mecânicas dos compósitos, testando diferentes concentrações de nZnO. Foram sintetizadas nanopartículas de óxido de zinco, através do método de precipitação química à temperatura ambiente, obtendo-se nano estruturas porosas. As membranas compósitas foram testadas contra E.coli e S.aureus evidenciando um bom comportamento antibacteriano, bem como uma relação do mesmo com a concentração de nZnO nas membranas. No que diz respeito aos ensaios mecânicos, as membranas mostraram boas propriedades.

Em conclusão, as nZnO podem ser adicionas ao PU formando uma membrana com propriedades antibacterianas e boas propriedades mecânicas.

keywords Composite membranes, Polyurethane, Zinc Oxide, Antibacterial properties, Mechanical properties, Vascular grafts.

abstract One of the great challenges of vascular tissue engineering (TE) is the lack of availability of autologous vascular tissues to replace small-diameter (<6 mm) blood vessels. Studies have shown that polyurethane has mechanical properties suitable for use in blood vessels of small diameters. Previous papers highlight the antibacterial properties of composites composed of PU and nanoparticles of zinc oxide (nZnO).

The present study had as objective the production of composite membranes of PU / nZnO with the use of electrofying. More specifically, it was intended to evaluate the antibacterial and mechanical properties of the composites by testing different concentrations of nZnO.

Nanoparticles of zinc oxide were synthesized through the chemical precipitation method at room temperature, obtaining nano porous structures. The composite membranes were tested against E. coli and S. aureus showing a good antibacterial behavior, as well as a relation thereof with the concentration of nZnO in the membranes. With regard to mechanical tests, the membranes showed good properties.

In conclusion, the nZnO can be added to the PU forming a membrane with antibacterial properties and good mechanical properties.

CONTENTS

LIST OF FIGURES

LIST OF TABELS

LIST OF ABREVIATIONS

BET	Brunauer, Emmet e Teller Surface Area
DMF	Dimetilformamida
DRX	Difração de Raio-X
DTA	Differential Thermal Analysis
ECM	Extracellular Matrix
IUPAC	International Union of Pure and Applied Chemistry
nZnO	ZnO nanoparticles
PU	Polyurethane
SSA	Specific Surface Area
SEM	Scanning electron microscopy
TE	Tissue Engeneering
TGA	Thermogravimetric Analysis
THF	Tetrahidrofuran
ZnO	Zinc Oxide

CHAPTER I

CONTEXT AND OBJECTIVES

1.1. Context

Vascular diseases are an important issue in modern times, being the number one cause of death, responsible for more than 17 million deaths worldwide [1] , resulting in an estimated cost of almost 196 billion euros a year in EU alone [2]. In Portugal, according to the Sistema Nacional de Saúde (SNS), vascular diseases account for 29.5% of the deaths recorded in 2013.

Therapies applied in clinical practice for treatment of vascular diseases include the transplantation of native autologous grafts, such as the saphenous vein or the internal mammary artery, the implantation of artificial grafts or the insertion of stents [3], [4]. However these clinical practices suffer from limitations. Although the use of autologous grafts shows good results, there is a lack of availability while inconvenient surgical harvesting and tissue graft preparation is required [3].

In case of donor grafts, the disadvantages are the shortage of available donors, the risk of pathogen transfer and rejection, and mandatory lifelong immunosuppressive therapies. Prostheses or devices re unable to completely restore the natural functions, often leading to unphysiological conditions which require permanent anticoagulation therapies [4]–[7]

Therefore, there is an urgent need to develop functional small diameter vascular grafts to replace diseased or narrowed blood vessels [8], [9].

The development of vascular bioengineering has led to a variety of novel treatment strategies for patients with cardiovascular diseases and today's major effort is focused on developing small diameter vascular grafts [10]. One of the strategic purposes of tissue engineering is to develop alternative materials that integrate with the patient's native tissue to restore its lost physiologic function.

1.2. Objectives

The present dissertation aims to develop PU/nZnO composites for vascular related diseases, to study its antibacterial behavior, as well as their mechanical properties. In this context, it is specifically intended to:

I. Synthesize zinc oxide nanoparticles (nZnO) with different characteristics by a chemical precipitation method at room temperature.
II. Optimization of the electrospinning parameters for the production of PU membranes
III. Produce PU/nZnO composite meshes by combining both components in different percentages
IV. Study the antibacterial behaviour of the PU/ZnO composites, trying to understand the impact of nZnO concentration on its bacterial response. A Gram-negative bacteria strain Escherichia coli (*E.Coli*) and a Gram-positive strain Staphylococcus aureus (*S.Aureus*) were tested.
V. Study the mechanical properties of the composite membranes, evaluating the effect of ZnO concentration on the membranes tensile strenght.

This dissertation is organized in five chapters.

The first chapter describes the context and the main goal of this work.

Chapter II is the State of the Art review, where the main problem proposed for this dissertation is addressed and a short review is made of the methods used to produce this type of membranes.

Material and Methods of the all work performed is presented in Chapter III.

Chapter IV presents all the results and discussion of the work. Finally, in the last chapter, the main findings of this dissertation and references to future prospects and possible improvements of this work are presented.

CHAPTER II

STATE OF THE ART

2.1. Blood Vessel Structure

Blood vessels present a complex structure which includes three different concentric layers, i.e. intima, media and adventitia, each of them with a different composition and function.

(1) Intima, the innermost layer, consists mainly of endothelial cells (ECs). It controls the molecular transfer inside the wall, providing antihormbogenicity. It is involved in homeostasis maintenance, muscular tone and immunogenic regulation;

(2) Media, the middle layer is composed mainly of circumferentially arranged layers of smooth muscle cells (SMCs), alternating with elastin sheets and collagen fibers. The SMCs are responsible for the regulation of vessel size and elastin sheets are responsible for the vessel's high compliance;

(3) Adventitia, the outer layer, consists of collagen fibers disposed in a circumferential orientation that anchor the vessel to its surroundings. Fibroblasts may also be present [11].

A representation of the blood vessel structure is shown in Fig 1.

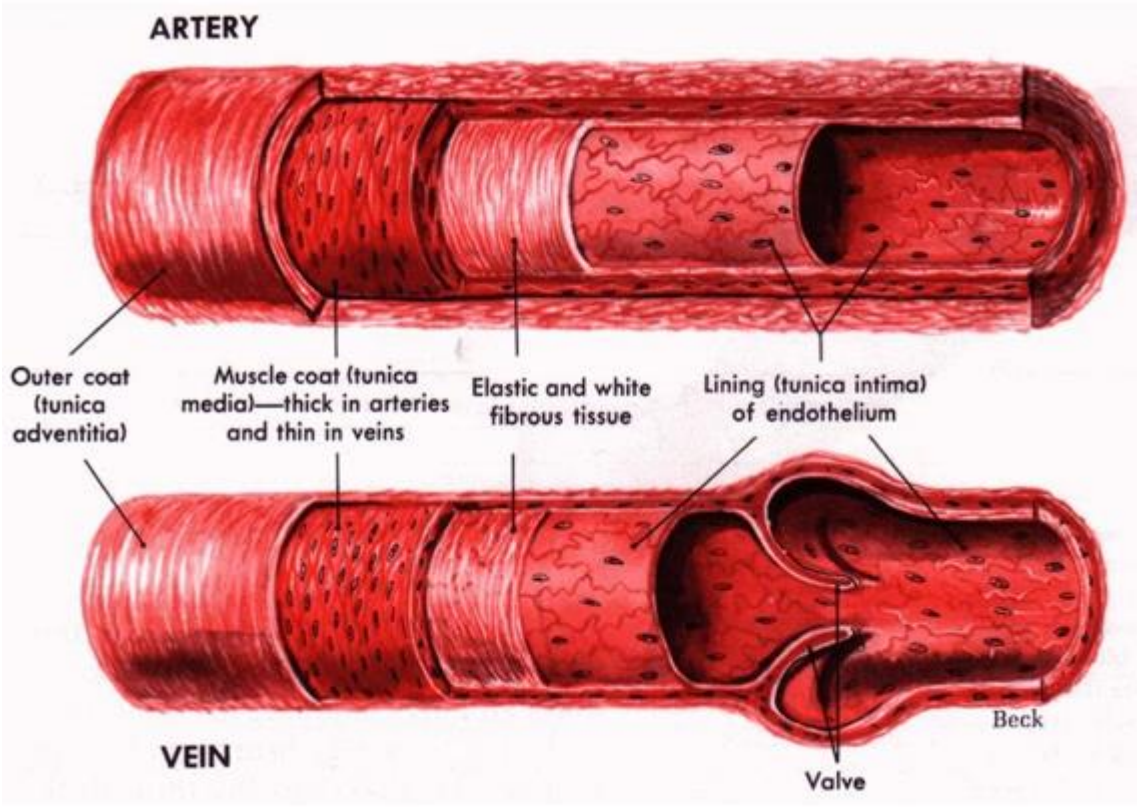

Fig 1: Blood vessel structure

The complex structure of blood vessels is not easy to mimic. A number of solutions have been proposed for blood vessels repair from natural and synthetic polymers to the TE approaches, although none has shown to be entirely satisfactory especially when low diameter vessels are needed.

2.2. Polymers in Vascular Tissue Engineering

Tissue engineering (TE) aims to develop alternative materials able to restore, maintain or improve patient's native tissue in order to reestablish its physiological function. Often it involves the use of synthetic or natural materials, denominated scaffolds, to provide a surface for cell growth and formation of a new tissue while degradation of the scaffold takes place [12].

Therefore, the traditional approach of te implies three contributions:

(1) From cells that synthesize the new tissue;

(2) From scaffolds that provide physical support to cells, and promote cell adhesion, migration, proliferation and differentiation;

(3) From biomimetic in vitro culture environments, which are designed to replicate in vivo conditions by using biological inspired requirements, aiming at inducing cell differentiation, and promoting extracellular matrix (ECM) formation and maturation [4], [13].

In the classical TE strategy, the scaffold should serve as a limited time device: being foreign to the natural environment, it should disappear once that function has been fulfilled, leaving behind a viable purely biological system. Therefore, the majority of the materials used in tissue engineering are biodegradable. In the design of biodegradable biomaterials, many important properties must be considered. These materials must

(1) not evoke a sustained inflammatory response;
(2) possess a degradation time matching their function;
(3) have appropriate mechanical properties for their intended use;
(4) produce non-toxic degradation products that can be readily reabsorbed or excreted;
(5) Include appropriate permeability and processability for specific applications.

The tissues of the human body are composed of two main constituents: cells, responsible for regulating body process and performing maintenance and wound healing, and ECM, the major structural component of the body. The ECM makes up a large majority of tissue volume, it consisting primarily of fibers with diameters between 50 and 500 nm [14]. The main goal of a scaffold is thus to mimic the advantageous characteristics of the ECM. The scaffold should be biocompatible, biodegradable and should meet the mechanical requirements suitable for its applications.

The architecture of scaffolds used for TE is of critical importance. Scaffolds should have an interconnected pore structure and high porosity to ensure cellular penetration and adequate diffusion of nutrients to cells within the construct and to the ECM formed by these cells. One of the major concerns is core degradation due to the lack of vascularization and waste removal from the scaffold. The pores need to be large enough to allow cells to migrate into the structure, where they eventually become bound to the ligands within the scaffold, but small enough to establish a sufficiently high specific surface area. A porous structure will allow the diffusion of waste products out of the scaffold, allowing products of scaffold degradation to safely exit the body [15].

The vascular environment is subjected to cyclic pressure imposed by the heart, which influences the behavior of tissue cells. Blood vessels must be distensible for easy adaptation to blood in circulation, but they must also be stable to inflations over a range of pressure, presenting a non-linear elastic behavior. An ideal tissue engineered vascular graft should possess vasoreactivity and biomemechanics similar to native vasculature [13]. The mechanical properties of the selected materials are thus key elements in the design of vascular TE. The implantation of grafts or prostheses will cause mechanical restrictions during the cardiac cycle [15].

Naturally occurring polymers, and synthetic biodegradable polymers are the main types of polymers used in vascular TE. Natural materials owing to its bioactive properties have better interactions with the cells which allow them to enhance the cell’s performance in biological systems. However their poor mechanical properties, high composition variability and fast degradation constitutes its most serious drawback. Examples of natural polymers used in vascular TE are shown in Fig 2 [3].

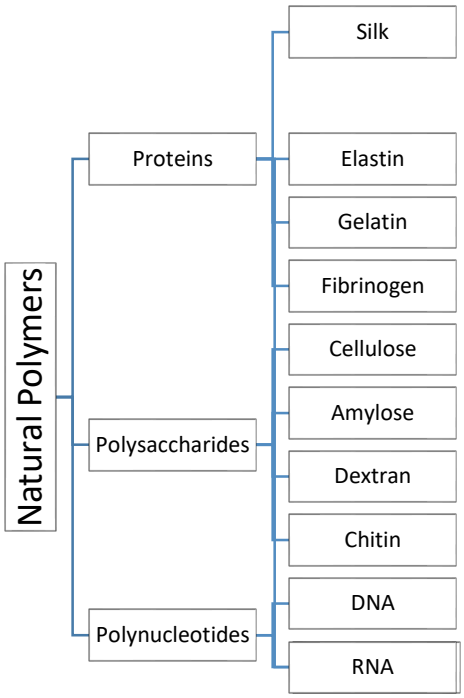

Fig 2: Examples of natural polymers used in Tissue Engineering

Synthetic biodegradable polymers are highly useful in TE, since their properties can be tailored for specific applications [12]. Synthetic biodegradable polymers can be produced under controlled conditions, exhibiting predictable and reproducible mechanical and physical properties, such as tensile strength, elastic modulus and degradation rate [12].

Examples of synthetic biodegradable polymers include poly(Ɛ-caprolactone), poly(L-lactide) and poly(glycolide).

Biodegradable polymers (BP) degrade via hydrolytic cleavage at the ester bond, producing fragments of low molecular weight. BP degradation is detected through the loss of mechanical properties, followed by the decrease of BP mass/volume. The rate of degradation of the polymer depends on its initial molecular weight and crystallinity, and on the exposed surface area [1].

2.3. Non degradable polymers for blood vessels grafts

Any artificial vessel substitute should ideally fulfill the following requirements:

(1) To be biocompatible and biostable: non-inflammatory, nontoxic, non-carcinogenic, and non-immunogenic;

(2) To be thromboresistant: to be impervious to blood, but to have adequate porosity;

(3) To remodel well, including easy regrowth of endothelium, which is a secretory tissue as well as a selective permeability barrier;

(4) To resist to infection;

(5) To be compliant (elastic): it must have appropriate mechanical properties;

(6) To be vasoactive: to possess appropriate vasoactive physiological properties including the ability to constrict or relax in response to neural or chemical stimuli;

(7) To offer a long-term tensile strength;

(8) To be of easy handling;

(9) To have suture holding strength, being able to allow sutures;

(10) To be easily available in appropriate specifications;

(11) To be easy to manufacture [3]

Natural polymers have been investigated for clinical applications as blood vessel substitutes due to their high biocompatibility but, their poor mechanical properties, high composition variability and fast degradation are as major drawbacks for vascular applications. Synthetic polymers were thus exploited. Among them, the polyester poly(ethylene terephthalate) (PET) and the fluoropolymer poly(tetrafluorethylene) (PTFE) have been highly used for the development of vascular grafts. PET (Dracon) and PTFE (Gore-Tex) were the first to obtain a FDA approval. Dacron, a thermoplastic polymer, consist of tubular structures of poly(ethylene terephthalate) and was first introduced in 1957. It has high crystallinity, high elastic modulus and tensile strength. Gore-Tex, which is expanded poly(tetrafluorethylene) (ePTFE), also presents high crystallinity and high stiffness, both lower than Dracon. Dracon and Gore-Tex show good results for application in grafts with internal diameter greater than 6 mm (between 7-9 mm).

However, both grafts fail in small diameter (<6mm) applications, mainly due to their poor blood patency rate, high stiffness and compliance mismatch [6], [7], [9], [13].

Altogether these factors result in an unavoidable thrombogenicity and an unsatisfactory prostheses performance for diameters smaller than 6 mm.

2.4 The chemistry of polyurethanes

Polyurethanes have been used as a biomaterial for many years, due to their mechanical properties, biocompatibility, and flexibility [16]. Traditional applications of PU involve catheter, transdermal patches, transient cardiovascular devices, among others [17]. PU vascular grafts can withstand the action of stress and load and undergo elastic recovery with little to no hysteresis. The high variability of PUs chemistry and their properties, allow the design of biocompatible material with controlled physical, chemical, mechanical and biodegradation properties, through the selection of the appropriate monomers and by manipulating hard and soft segment contents[18]. These polymers are characterized by the presence in their chain of one or more urethane linkages. The urethane linkage established by the reaction between the two basic components of polyurethane, a polyol and an isocyanate. This type of link was first discovered in 1849 when Wurtz and Hoffman studied the reaction between an isocyanate and a compound with alcohol functional groups. Figure 3 describes the reaction between an isocyanate and a polyol.

As represented in Fig 3, polyurethane (PU) is formed from two precursor compounds, the polyol and diisocyanate (4,4′-MDI) which will be addressed in the next sub- sections A third compound might be used as a chain extender, usually a diol or amine (Figure 3) [19].

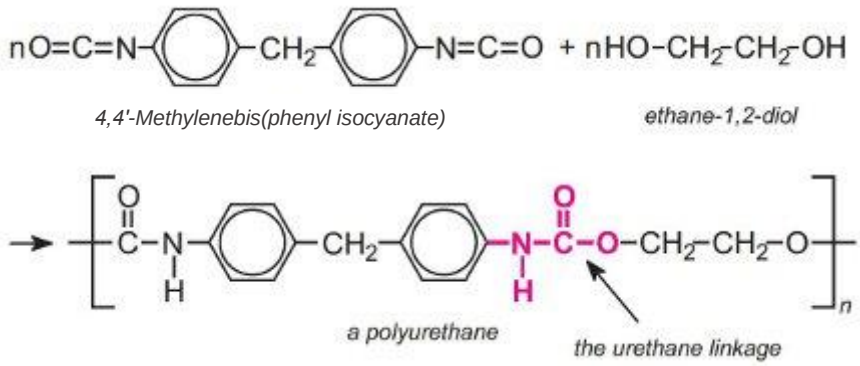

Fig 3: Schematics of polyurethane synthesis

Polyol

Conventional polyols are either a polyether or a polyester (-R-O-R'- or -R-COO-R'- respectively), with a hydroxyl termination. When aliphatic polyols and low intermolecular interactions are concerned, polyols are flexible, and consequently are referred to as flexible portion of the PU. Polyethers are more hydrolytically stable than polyesters, and are usually used when high flexibility and extensibility are needed [20].

Table 1 shows a list of the most commonly used polyether and polyesters.

Table 1 - Examples of most commonly used polyether and polyesters.

Polyether	**Polyester**
Poly(ethylene oxide) (PEO) 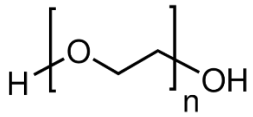	Poly(ε-caprolactone) (PCL) diol 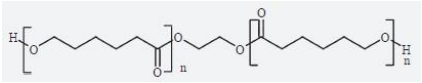
Poly(propylene oxide) (PPO) 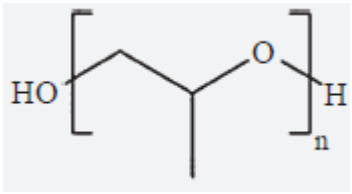	Poly(d,l-lactide) (PDLLA) diol 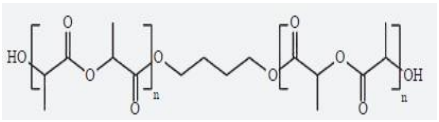
Poly(tetramethylene oxide) (PTMO) 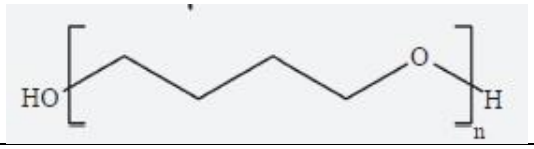	Poly(glycolide) (PGA) diol 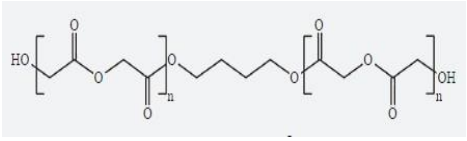
Poly(hexamethylene oxide) (PHMO) 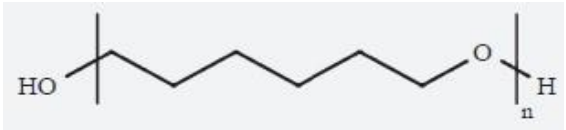	Poly(ethylene adipate) diol 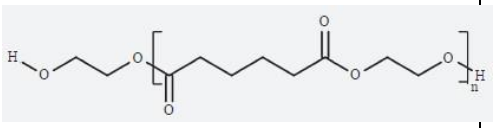

Isocyanate

The two main classes of isocyanates used to generate biomedical polyurethanes are aromatic and aliphatic. The most important isocyanate used in the synthesis of the polyurethane is the diisocyanate, which contains two isocyanate groups per molecule.

An example is shown in Fig 4 where we can see the representation of Lysine methyl ester diisocyanate (LDI) with two isocyanate groups highlighted.

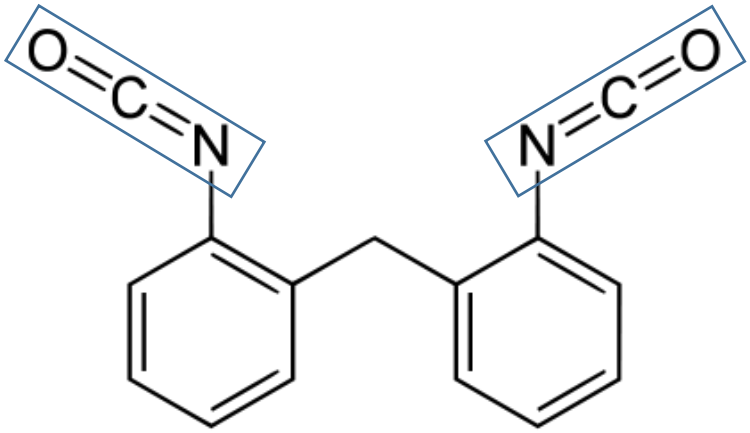

Fig 4: Lysine methyl ester diisocyanate (LDI) and Methylene diphenyl diisocyanate (MDI)

These two functional groups have the function of linking, through a chemical reaction, the two other molecules required for the synthesis of a PU (two polyols, or a polyol and a chain extender) forming a linear chain. When the functionality of the isocyanate is greater than two, a linkage between molecules can be established, leading to the formation of a crosslinked network. Due to the ring shaped structure of the diisocyanates, and due to their strong intermolecular interactions, the resulting chain in this case is referred to as the rigid chain of the PU. Amongst the most used diisocyante structures one can cite: 1,4-Diisocyanatobutane (BDI); 1,6- Diisocyanatohexane (HDI); Lysine methyl ester diisocyanate (LDI) and Methylene diphenyl diisocyanate (MDI) [18].

Chain Extenders

Chain extenders are low molecular weight diols or diamines that react with diisocyanates to build polyurethane molecular weight and increase the block length of the hard segment. Chain extenders made from diols such as ethylene glycol, butane diol, and propylene glycol result in a urethane linkage [21], [22].

The use of diamine chain extenders results in a urea linkage. They are associated to increased modulus and tensile strength and to decreased elongation of PU, as compared to their diol counterparts [23].

2.5 Polyurethanes for vascular repair

Polyurethanes (PU) appeared as alternative graft materials due to their biocompatibility and mechanical properties, especially low temperature flexibility, abrasion resistance, controllable stiffness and fatigue resistance, which offer a very good match to the native vascular tissue [24]. Additionally PUs are not expensive and are easily processed.

These same properties have allowed the application of PU in the biomedical industry since the 1960s [25]. PU are currently used in the production of heart valves, blood storage bags, dialysis membranes, prostheses, bone adhesives, sutures and drug controlled release systems [26].

Different manufacturing techniques can be used to produce the PU structures depending on the envisaged morphology. Recently electrospinning appears as a very a versatile technique allowing the production of nanofiber membranes with a microstructure that closely resembles the ECM.

Several studies are reported on the production of PU membranes for different applications. A review of some of those studies is presented bellow and details on the electrospinning technique used in the meshes fabrication are presented in

Eectrospinning was used to pattern the luminal surface of small-diameter PU grafts, prepared from aromatic commercial PU (Tecothane) with microfibres and microgrooves was developed [27]. The biocompatibility of the designed grafts was measured by seeding its patterned luminal surface with endothelial cells and then following their growth and orientation on this surface. Uttayarat et all [27] concluded that the micropatterned vascular

grafts were able of promoting the formation of aligned and cytokine-responsive endothelial monolayers.

A PU surface modification was proposed by Blit et al.[28], who used elastin cross-linked peptide (ECP) to modify PU surface. The PU matrix was obtained from poly(hexamethylene carbonate) diol (Mw= 860), 1,6-hexamethylene diisocyanate (HDI) and 1,4-butanediol (BDO) as chain extender. The surface of the obtained electrospun PU scaffolds, with fibrous structure, was modified by recombinant elastin-like polypeptide-4 (ELP4). The prepared scaffold was used as a support for vascular smooth muscle cells (SMCs) adhesion and then examined. Scaffold surface modification by ELP4 caused the enhancement of the cells adhesion and proliferation thus improving PU biocompatibility.

The effect of solvent ratio (DMF/ THF) (Dimethylformamide/Tetrahydrofuran) and rotational speed on the mechanical properties of electrospun grafts obtained from poly(ether urethane) (SPEU) was studied by Matsuda et al. [29]. It was observed that an increase of the DMF/THF ratio led to fiber fusion and to a decrease in fiber diameter, leading to lower compliance values [29]. An increase of the rotational speed led to stiffer, less compliant tubes. Another study confirmed that an increase in the DMF/THF ratio significantly increased fiber bonding and elastic modulus.

Carbothane® PC3575A (Carbothane, Lubrizol), a poly(carbonate urethane) (SPCU) containing MDI and HMDI, respectively was tested by Nezarati et al [30] to evaluate its mechanical behavior on a vascular graft application. Due to its content of aliphatic hard segments, Carbothane® had a lower initial Young's modulus, and an increased compliance, and was used for the fabrication of an electrospun vascular graft. Fiber fusion generated by heat treatment led to vascular grafts with both compliance and burst pressure exceeding saphenous vein's autografts.

Eectrospun grafts obtained from poly(ether urethane) (SPEUs) were prepared by Cozzens et al, [31] using hydroxypropyl telechelic polyisobutylene (PIB) and polytetramethylene oxide (PTMO) (80:20) as soft segments, and MDI and Butanediol (BDO), with variation of the ratio of the hard segments. The obtained SPEUs were electrospun as flat meshes and displayed higher mechanical properties than native vessels, suggesting that they are promising materials for the production of biostable vascular grafts. An increase of the Young's modulus and tensile strength was observed.

Han et al. [32] synthesized a SPEsUU from PCL, l-lysine ethyl ester diisocyanate (LDI), and l-lysine ethyl ester (LEE) as chain extender. The mechanical properties of the electrospun tubular scaffolds were dependent of the solution concentrations, as a higher concentration leads to a higher diameter, and therefore enhance mechanical properties.

The values of suture-retention strength were higher than those of native blood vessels, whereas the burst pressure strength was slightly lower.

Another important aspect of the development of vascular tissue engineering is bioresorbability/biodegradability of PUs.

Using polycaprolactone diol (PCL-diol) (Mw = 1250), 2,6-diisocyanate methylcaproate (LDI) and L-phenylalanine-based diester chain extender for the PU synthesis, Rockwood rt al tried to increase the biodegradability of the electrspun isotropic PUs scaffold (ES-PU). As it is commonly known PU formed from polyester polyols is more susceptible for degradation than polyether polyols. The authors concluded that the physical organization of microfibres in ES-PU scaffolds impacts both multi-cellular architecture and cardiac cell phenotype in vitro. Isotropic and aligned microfibrous templates were capable to support primary cardiac cell cultures in a serum free medium.

Polyurethanes (PUs) of increased biodegradability were prepared by Han et al [33] through synthesis of poly(ε- caprolactone)diol (PCL) with two different molecular masses: Mw = 2000 and Mw = 1250, which reacted with L-lysine ethyl ester diisocyanate (LDI). The PU membrane, obtained via electrospinning, displayed enhanced tensile strength, burst pressure strength and suture retention strength. In general, the physico-mechanical parameters were improved with increasing solution concentration of PU. The cytotoxicity and cell adhesion were measured with the use of L-929 fibroblast cells and HUVECs. The results revealed that the obtained scaffolds provided cells proliferation and adhesion, proving that material may serve as blood vessel graft. Using naturally occurring peptides, such as elastin, which participate in ECM formation and tissue remodeling, the probability of healthy soft tissue reconstruction is increased.

To study the effect of porosity on cellular growth and migration Bergmeister et al.[34]. prepared Pellethane® small-diameter vascular grafts. It was observed that grafts with higher porosity exhibited higher cell attachment after implantation; while the values of compliance and tensile strength remained higher compared to native blood vessels for grafts before and after 6 months of implantation in rats. Pellethane® usage has been restricted to short term periods due to its biodegradability in long-term applications.

To avoid clot formation due to thrombogenicity it is also important to focus on the PU surface. The main approach employed is by modification of PU's membranes surface, usually by incorporation of compounds such as heparin or nitric oxide, both known for their aintithrombogenic properties [35].

With the growing public health awareness associated with the pathogenic effects caused by microorganisms, there is an increasing need for antibacterial materials in many application areas like medical devices and health care in general. Although PU membranes exhibit quite adequate properties for vascular grafts applications, they lack antibacterial activity. Specific additives or fillers may be blended with the PU matrix in order to induce this biocide ability.

Zinc oxide nanoparticles are of great interest in the biomedical field due to its antibacterial activity. The possibility of filling PU membranes with ZnO nanoparticles appeared as quite adequate. Despite all reported investigations on the interactions between cells and nanoscale surfaces of biomaterials, to our knowledge the antibacterial behaviour of electrospun ZnO-added PU membranes, has not been studied so far.

2.6 Zinc Oxide

ZnO may be described as a functional, promising and versatile inorganic material with a broad range of applications. Due to the Zn and O position on the periodic table (groups II and XI respectively), ZnO holds unique optical, chemical, semiconducting and piezoelectric properties which allow ZnO to have a wide range of applications across many different fields such as sensors, transducers and catalysts [36].

Crystal structure of ZnO and particles morphology

Zinc oxide crystals possess a wurtzite structure at ambient conditions. As seen in Fig 5**Erro! A origem da referência não foi encontrada.** The structure is composed of two interpenetrating hexagonal closed packed (HCP) sublattices, each of them consisting of one type of atom (Zn or O) displaced along the c-axis. Each Zn atom is surrounded by four oxygen atoms and vice-versa. The ZnO structure can be explained as a number of alternating planes stacked layer by layer along the c-axis direction and composed of

tetrahedrally coordinated Zn^{2+} and O^{2-} with lattice parameters a = 0.3296 and c = 0.52065 nm. The structure is thermodynamically stable in an ambient environment [37].

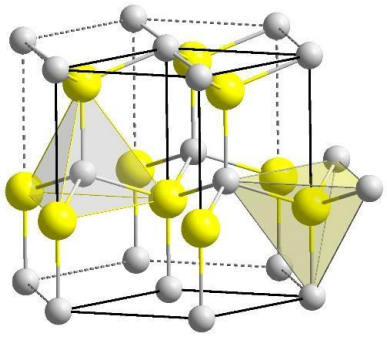

Fig 5: Zinc Oxide structure

ZnO particles can be produced with different sizes and shapes. The nanoscale size usually confers large surface area to nanoparticles, compared to macrosized particles. Nanoparticles show size related properties significantly different from those of bulk materials. Given the versatility of their properties the small size, nanoparticles applications are very broad and can range from biosensors to nanomedicine [38].

Due to the great potential of ZnO in many fields, various synthetic methods have been used to grow a variety of ZnO nanostructures, such as nanoparticles, nanowires, nanorods, nanotubes and other complex morphologies. Depending on the final application, different methods are available to produce different morphologies. and properties as resumed in Table 2 [39].

Table 2 - Different processes to synthesize ZnO nanoparticles

Author	Techniques	ZnO morphology
Jalal et al.	Microwave decomposition	**Sphere**
Ramani et al,	Simple wet chemical route	**Nano and micro-flowers, rice flakes and rings**
Kumar et al	Simple precipitation method	**Nano-flakes**
Stankovic et al	Hydrothermal synthesis	**Hexagonal prismatic rods**
Talebian et al.	Solvothermal method	**Nano-flowers, nano-spheres**
Ma et al.	Microwave hydrothermal method	**Mulberry-like**
Hafez et al.	Hydrothermal technique	**Nanorods**
Chen et al	Chemical precipitation	**Nano-flakes**

In the present work, ZnO will be obtained through chemical precipitation at room temperature, as will be later detailed in Chapter 3. This technique presents several advantages, mainly its low cost, as it can be performed at room temperature and does not require expensive reagents or complex equipment [40].

Antibacterial Properties of ZnO Nanoparticles

Antibacterial agents are of great relevance to a number of industrial sectors, including environmental, food, synthetic textiles, medical care among many others. Antibacterial agents can be classified as, organic and inorganic [41]. Organic agents, possess a drawback as they are less stable at higher temperatures when compared to inorganic ones. Inorganic agents are mainly composed of metal and metal oxides, such as Ag, TiO_2, ZnO, MgO and CaO. Some of these oxides are part of essential minerals for human

health (MgO and CaO), while others have been used extensively in the formulations of personal care products [42].

Metal oxides nanoparticles represent a new class of important materials with a recent increased use in health related applications. ZnO powder has been used as an active ingredient for dermatological applications in creams and lotions due to its antibacterial properties [43]. On a nanoscale ZnO nanoparticles can interact with bacterial surface and bacterial core, resulting in toxic interactions. However, ZnO nanoparticles have proven to be non-toxic for human cells.

Several studies have already been performed, proving the antibacterial properties of ZnO nanoparticles, while establishing a relation between the size of the particles and their antibacterial properties.

Different methods have been adopted for the assessment and investigation of the *in vitro* antibacterial activity of ZnO alone or combined with other components. These methods include disk diffusion, broth dilution, agar dilution, and the microtiter plate-based method.

Li et al studied the effect of ZnO nanoparticles on the mechanical and antibacterial properties of PU thin films, prepared by solvent casting and evaporation technique [36]. ZnO nanoparticles were obtained through coprecipitation using $Zn(O_2CCH_3)_2{\cdot}2H_2O$ and $(NH_4)2CO_3$ as precursor reagents and the obtained crystals, with hexagonal structure exhibited an average size of 27 nm. The Young modulus of the ZnO-PU composite film, as compared to pure PU films, appeared to increase with the ZnO concentrations up until 2 %, a further increase of concentration resulted in a decrease of the tensile strength as seen in Table 3.

Table 3 - Mechanical properties, (Young's modulus and tensile strength) of composite ZnO-PU films obtained by solvent casting.

ZnO (wt%)	Young's modulus (MPa)	Tensile strength (MPa)
0.0	517,42	8,58
1.0	660,34	16,74
2.0	710,48	17,83
3.0	557,7	10,42
4.0	512,76	7,24

The same authors reported the results of antibacterial tests with the ZnO-PU composites performed according to the agar dilution method against *E. coli* and *B. subtilis* The results indicated that the composite films possess excellent antibacterial property and the increasing antibacterial efficiency correlates with the increase of ZnO content. A higher efficiency against *E. coli* as compared to *B. subtilis* was observed [43].The anti-bacterial properties of several metal oxide nanoparticles were also studied by Jones et al [44]. ZnO nanoparticles (50 - 70nm), obtained from Sigma-Aldrich, were suspended in sterile double-distilled water. Turbidity as a qualitative measure was used to examine the anti-bacterial activity, at 600nm. The results showed that for the tested concentration (1nM) ZnO nanoparticles produced a 95% growth reduction of *Staphylococcus aureus*, while ZnO ultrafine powder (average size >1µm) only produced 50% of growth reduction, proving that the antibacterial activity has an important dependence on the particle size.

Together with particle size, concentration of particles in the antibacterial medium also revealed to have major importance. Commercial ZnO particles with sizes in the ranges 24-71 nm and from 90 - 200nm have been tested by Zhang et al against E. coli growing in a Luria-Bertani (LB) medium. Antibacterial tests were performed by measuring the growth curve of *E. coli* incubated in the LB broth medium in the presence of the nanofluids containing different concentrations of ZnO nanoparticles. The results showed that the antibacterial activity increased with the increasing particle concentration and the decreasing particle size, being the particle concentration more significant than the particle size particle size under the conditions of this work [42].

As shown in the literature ZnO shows antibacterial behavior against either Gram positive or Gram negative bacteria. It is accepted that this behavior results from the binding of ZnO particles to the cell membrane of the bacteria, damaging it, as a result of the production of reactive oxygen species (ROS) which plays a very important role in the disorganization and disruption of this membrane [45].

The term reactive oxygen species (ROS) is used to refer free radicals derived from molecular oxygen. They can be the byproduct of several biological processes, and can be harmful for the cell. In the case of zinc oxide, the reactive species are hydroxyl anion (OH^-), superoxide anion (O^{2-}) and hydrogen peroxide (H_2O_2) which can be formed by several routes, namely the photocatalysis on the surface of a particle (Fig 6). Under action of UV or visible radiation, whose energy is higher than 3.3 eV, electrons from the ZnO valence band move to its conduction band. Thus they form holes (h^+) in the valence band and free electrons (e^-) in the conduction band (equation a, Fig 6). The h^+ holes react with the water present in the medium producing H^+ and $^{\cdot}OH$ (equation b, Fig 6), the electrons react with the oxygen, also present in the medium, giving rise to the superoxide anion $\cdot O_2^-$ (equation c, Fig 6), which in turn reacts with H^+ to give the hydroperoxyl $\cdot HO_2$ radical (equation d, Fig 6). This radical then reacts with another free electron producing the hydrogen peroxide anion HO_2^- (equation e,Fig 6), which will react with the H^+ ion leading to the formation of the hydrogen peroxide molecule H_2O_2 (equation f, Fig 6) [46].

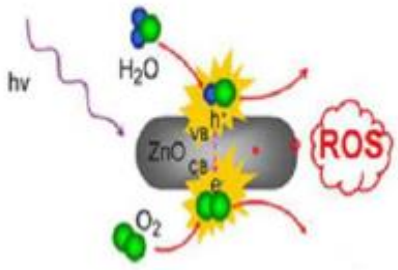

$$ZnO + UV \longrightarrow e^- + h^+ \quad (a)$$

$$h^+ + H_2O \longrightarrow H^+ + {}^{\cdot}OH \quad (b)$$

$$e^- + O_2 \longrightarrow {}^{\cdot}O_2^- \quad (c)$$

$${}^{\cdot}O_2^- + H^+ \longrightarrow {}^{\cdot}HO_2 \quad (d)$$

$${}^{\cdot}HO_2 + e^- \longrightarrow HO_2^- \quad (e)$$

$$HO_2^- + H^+ \longrightarrow H_2O_2 \quad (f)$$

Fig 6: Mechanism of action for different types of ROS produced by ZnO

The toxicity of ROS is attributed to their high reactivity and oxidation capacity, which results in the destruction of cellular components such as lipids, DNA and proteins [47]. Literature reports that the action of ROS can lead to loss of cell membrane integrity, resulting in dysfunctionalities in the permeability barrier, which will result in the death of the cell. The ROS mechanism begins with the release of oxygen species from the surface of the particles, which react with the cell membrane, causing its rupture through lipid peroxidation, exposing the cellular content. ROS can then penetrate into the cell and react with nucleic acids and proteins [48].

ROS can be quantified for example by the amount of glutathione in its oxidized form (GSSH). Glutathione ($C_{10}H_{17}N_3O_6S$) is a non-enzymatic, water-soluble antioxidant, and is recognized as the most important non-protein thiol in living systems. It is a linear tripeptide, consisting of three amino acids: glutamic acid, cysteine and glycine. It exists in most cells at concentrations ranging from 1 to 8 mM and may be in reduced (GSH) or oxidized form (GSSH). The importance of this pair is such that the GSH / GSSH ratio is normally used to estimate the oxidative state of biological systems [48].

2.6 Electrospinning

Currently, nanofibers have attracted tremendous attention due to their enormous potential for a wide range of applications. The most growing applications include filtration, tissue engineering, biomaterials, nanocomposites, and drug delivery[49]. Among the several approaches for the preparation of fibers, electrospinning has emerged as a straightforward and cost-effective technique for the convenient fabrication of nanosized to microsized fibers from a variety of materials [6].

The electrospinning phenomenon was first observed by Rayleigh in 1897, and was patented in 1934 by Formhals [50]. Since then several upgrades have been made to the equipment design and applications, such as the use of polymer for biomedical applications. Electrospinning relays on the electrostatic force to create fine fibers from a polymer solution. The electrospinning equipment is simple and comprises a syringe pump, a syringe with a metal needle loaded and with a polymer, a conductive collector and a high voltage supply (Fig 7) [51].

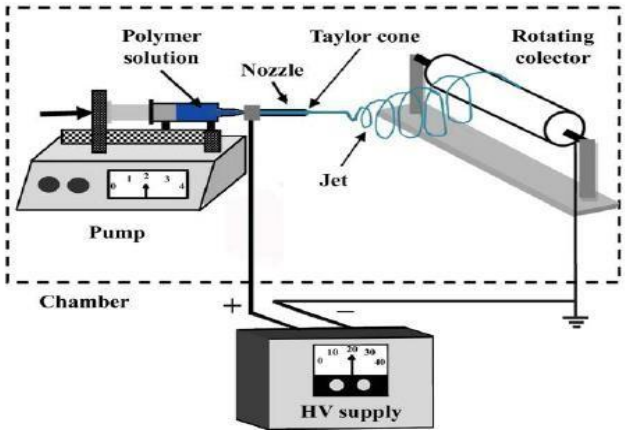

Fig 7: Schematics of the Electrospinning equipment

The high voltage will charge the polymer solution leading to the starching of the liquid, forming the Taylor cone. The induced electrostatic repulsion will reach a critical value that will overcome the surface tension of the liquid, and the polymer solution and then travels toward the charged collector as the solvent evaporates. The dried polymer fibers deposit onto the collector as randomly oriented or aligned pattern of fibers, depending on the type of the collector.

Table 4- Electrospinning parameters gathered from previous studies

Author	Solvent	Concentration	Voltage	Flow Rate	Objectives
Amna et al.	DMF, THF	NA	20 kV	NA	Vascular grafts
Blit et al	HFIP	16 wt%	12kV	0,5 ml/ h	Increase PU degradation
Caracciolo et al	HFIP	5-30 wt%	10-20 kV	0,5- 3 ml/ h	Soft tissue Eng.
Chen et al	HFIP	6 wt%	20kV	0,8- 1,2ml/ h	Vascular grafts
Courtney et al	HFIP	5 wt%	15 kV	1,0 ml/ h	Scaffold production
Gluck et al	HFIP	5 w/v %	28kV	0,07 ml/ h	Scaffold production
Grasl et al	HFIP	5 wt%	20kV	NA	Vascular grafts
Han et al	HFIP	5 w/v%	15kV	0,8 ml/ h	Increase PU biocompatability
Huang et al	HFIP	6 w/v%	15 kV	1 ml/ h	Vascular grafts
Matsuda et al	THF; DMF	15 wt%	30 kV	NA	Small dimention grafts
Milleret et al	HFP/ Chloroform	15- 25 wt%	15 kV;	NA	Vascular grafts
Rockwood et al	DCM	18 w/v%	1-15 kV	1,5 ml/ h	Limit peptid expression
Soletti et al	HFIP	8 w/w%	10 kV	NA	Vascular appilcations
Uttayarat et al	HFIP	5 w/v%	12 kV	0,8 ml/ h	Vascular grafts
Wang et al	THF; DMF	10 w/v%	18 kV	NA	Increase hemocompatability
Williamson et al	DMF	20 w/w%	12- 15 kV	NA	Vascular tissue scaffolds
Youan et al	DMF, THF	10 w/v%	16kV	0,6 ml/ h	Vascular grafts

Electrospinning operative conditions

The efficient operation of the electrospinning equipment requires the observation of some parameters and characteristics of the solutions, which are detailed below.

Voltage

It is known that the flow of current from a high-voltage power supply applied into a solution via a metallic needle will cause a spherical droplet to deform into a Taylor cone and form ultrafine nanofibres at a critical voltage, determined by the type of polymer. Although drops may form at relatively low voltage, voltage increase will produce fibers with reduce diameter, due to the stretching of the polymer solution which correlates with the charge repulsion within the polymer jet. However, when the voltage is too high, the process becomes unstable. Thus, an optimum voltage is required for a stable electrospinning process [52].

Flow Rate

The flow rate of the polymer solution is very important in the electrospinning process; it is regulated by the syringe pump. Usually, increasing the flow rate will originate an increase in fiber diameter and a slow flow rate may induce a temporary break in the electrospinning process. Polymer drops may form when the flow rate is too high as the fiber production rate cannot keep up with the flow rate. The ideal situation is that a stable Taylor cone forms during electrospinning, and the fiber formation rate is equal to the infusion rate, resulting in a stable process [51].

Effect of needle to collector distance

The distance between the needle tip and the collector is usually a neglected parameter. The distance is related to the solvent evaporation and the electrostatic force. Increasing distance will lead to a better evaporation of the solvent giving thinner fibers. Shorter distances will originate thicker fibers as the solvent may not evaporate completely, it may also lead to increased fiber fusion [51].

Tip Diameter

The tip diameter is closely related to the formation of a stable Taylor cone, but it does not affect the fiber diameter [50].

Effect of polymer concentration

Altering the polymer concentration is an effective way to optimize the fiber diameter. The polymer concentration is associated to the viscosity of the solution an increase of polymer concentration will lead to an increase in the viscosity of the solution and will originate a large fiber diameter; on the other hand, lower concentration will lead to the formation of polymer beads as continuous polymer fiber cannot be achieved. Thus, an appropriate polymer concentration is very important to the process of electrospinning [50].

Solvent

The main requirement for an electrospinning solvent is high volatility, as the solvent should evaporate quickly. Another important parameter is its electrical conductivity: a highly conductive solvent will produce thinner fiber diameters, and a polymer solution with low conductivity tends to form drops during the process [50].

Polymer properties

The overall structure of the polymer will affect the fiber formation. Polymers must be soluble in the organic solvent. Hence, crosslincked polymers and some linear polymers with high crystallinity cannot be electrospun. The molecular weight affects the rheological and electrical properties of the polymer solution such as viscosity, surface tension and conductivity. Generally, the fiber diameter increases with increasing polymer molecular weight. Low molecular weight will result in a small number of polymer chain entanglements in the solution, resulting in increased difficulty for the polymer chains to form fibers [50].

For the case of PU fibrous membranes produced by electrospinning, a resume of the experimental conditions used by different authors is presented in Table 4.

CHAPTER III

MATERIALS AND METHODS

In the present chapter, the procedures and techniques used in this study will be described. The first sections refer the used materials and reagents, as well as the techniques employed in the synthesis of zinc oxide nanostructured particles (nZnO) and in the preparation of the composite membranes of PU and zinc oxide (PU/ZnO) composites.

Briefly, nZnO were synthesized by a chemical precipitation method, using different concentrations of reagents and different addition rates of reagents, in order to produce a wide range of particles, from which the one with larger specific surface area was chosen.

The experimental protocol for carrying out antibacterial activity tests is also described below. A brief report of all the characterization techniques used throughout this work is presented as well.

3.1. Materials and Reagents

In the following table (Table 5) are presented the materials and reagents used in the synthesis of ZnO nanoparticles and in the production of composite membranes, and respective purity and commercial supplier.

Table 5 - Materials and reagents used in the synthesis of ZnO nanoparticles and in the production of PU/ZnO composites.

Reagents	Chemical Formula	Supplier	Purity
Citric Acid Monohydrated	$C_6H_8O_7.H_2O$	Sigma-Aldrich	>99.5
Zinc Chloride	$ZnCl_2$	Aldrich	-------
Absolute Ethanol	C_2H_5OH	Carlo Erba	>98
Sodium Hydroxide	NaOH	Sigma-Aldrich	>98.5
Polyurethane	PU	Sigma-Aldrich	-------
Tetrahydrofuran	C_4H_8O	Carlo Erba	-------
Dimethylformamide	C_3H_7NO	Carlo Erba	-------

3.2. Synthesis of Zinc Oxide Nanoparticles

Zinc oxide nanoparticles were synthesized using a chemical precipitation method at room temperature, as described in the literature and optimized by previous works developed at the Department of Materials and Ceramic Engineering of the University of Aveiro [53].

The method is based on the addition of a basic solution (sodium hydroxide) to an acidic solution of zinc ions (Zn^{2+}) (i.e zinc chloride acidified with citric acid). The resulting precipitate is a white powder composed of zinc oxide nanostructured particles (nZnO).

In the following scheme (Fig 8) is represented the overall process used in the synthesis of nZnO.

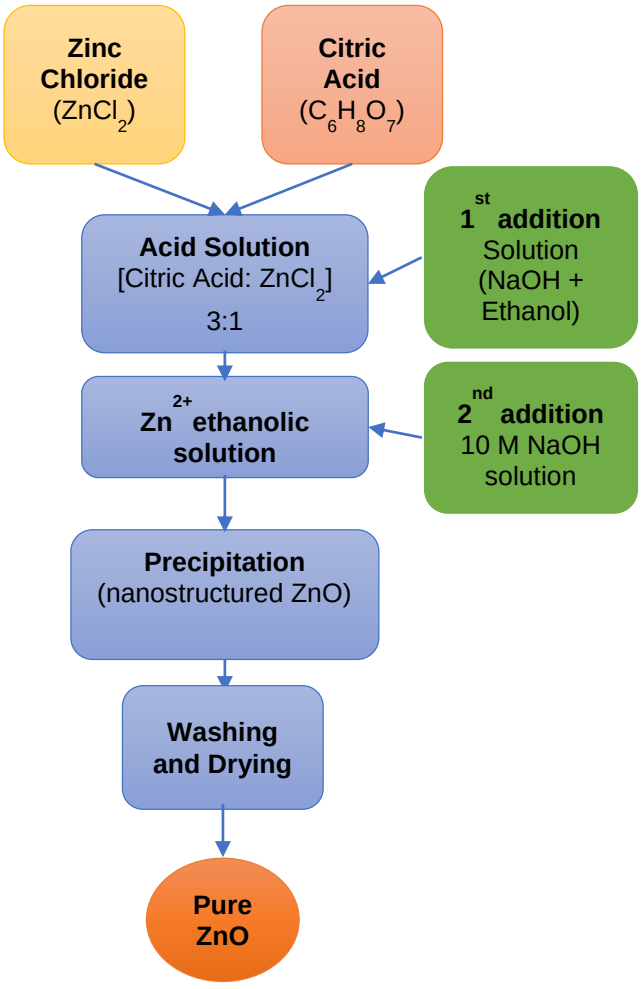

Fig 8 - Flowchart for the production of ZnO nanoparticles via chemical precipitation

.

The additions of the basic solution to the acidic solution of Zn^{2+} were made using a burette. The schematic of the used apparatus is presented in Fig 9.

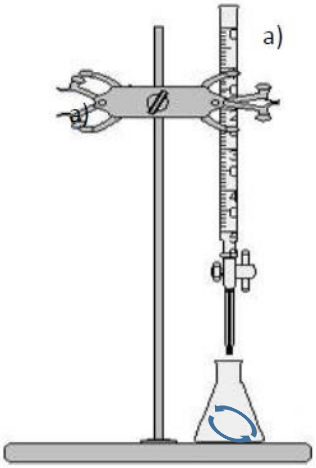

Fig 9 - Schematics of the apparatus used in the production of ZnO nanoparticles: the hydroxide solution contained in the burette was dropped over the acidic solution of the cation inside the bottom Erlenmeyer

In this study, several types of ZnO powders were produced Table 6. The only difference in the synthesis method was the ratio between Citric Acid (Cit) and Zinc Chloride, and the flow rate of the added solution to the bottom Erlenmeyer.

Table 6 - Different conditions used for the production of ZnO nanoparticles

nZnO label	Addition rate (mL/min)	(Cit:Zn^{2+}) molar ratio
nZno 1	18	2.7:1
nZno 2	13	3:1
nZnO 3	11	3:1
nZnO 4	10	3:1
nZnO 5	16	3:1

Three solutions (solution 1, 2 and 3) were prepared for the synthesis of the ZnO nanoparticles: two basic solutions and an acid solution.

Solution 1 consists of sodium hydroxide (NaOH) (10 M concentration) dissolved in distilled water (H_2O), under magnetic stirring (30 rpm) for 5 minutes.

The pH value of this solution was approximately 14.

The preparation of the acidic Zn^{2+} solution (Solution 2) was made mixing Monohydrated Citric Acid and Zinc Chloride ($ZnCl_2$) in distilled water, under magnetic

stirring. The pH of this solution was approximately 1. The Zn^{2+} ion concentration of this solution was 1.16 mol/ L and 1.07 mol/ L for nZnO-1 and nZnO-2, respectively.

Solution 3 was prepared by mixing the ethanol and the sodium hydroxide solution in a ration of 1,3:1 (hydroxide solution : ethanol).

The quantities of reagents used in the preparation of solutions 1 and 2 for the synthesis of the two types of zinc oxide powders, ZnO-1 and ZnO-2, are summarized in Table 7.

Table 7 - Quantity of reagents used in the preparation of the solutions for the nanoparticles synthesis.

	Solution 1	**Solution 2**	
	NaOH (mmol/ml)	Citric Acid (mmol/ml)	ZnCL2 (mmol/ml)
nZnO-1	10	2.86	1.16
nZnO-2	10	3.24	1.06

The solution 2 was placed in the Erlenmeyer under constant magnetic stirring.

Solution 3 was then added through the burette, followed by the addition of the solution 1. As a result of this process a suspension of nZnO is obtained, with a pH of approximately 13.

The nZnO suspension then undergoes 10 cycles of centrifugation at 10000 rpm for 10 minutes. The resulting sediment is washed with distilled water after each cycle. The washing cycle's main goal is the elimination of sodium ions (Na+) for obtaining pure zinc oxide.

Finally the precipitate was dried overnight in an oven at 60ºC.

All the precipitated powders were observed by scanning electronic microscopy (SEM) on a SU-70 Hitachi equipment. Crystalline phase composition and crystallite size were evaluated by x-ray diffraction (XRD) analysis on a PANalytical X'PertPRO diffractometer in a $20º<2\Theta<80◦$ range.

Elemental phase composition was confirmed by the Energy Dispersive Spectroscopy (EDS) equipment coupled to the electronic microscope. Specific surface area, and pore size distribution were determined by gas (N_2) adsorption based on Brunauer-Emmett-Teller (BET) isotherm using a micromeritics datamaster equipment. The used degasification temperature was 100ºC for 16h.

3.3. Pu/ZnO Membrane production and characterization

Several composite samples (0, 10, 25 and 50% mass of ZnO in regards to the mass of PU) were produced using the electrospinning technique (Fig 10). The different concentrations of nZnO were chosen to study the effects of nZnO concentration in both the mechanical and the anti-Bacterial properties of the composite membrane.

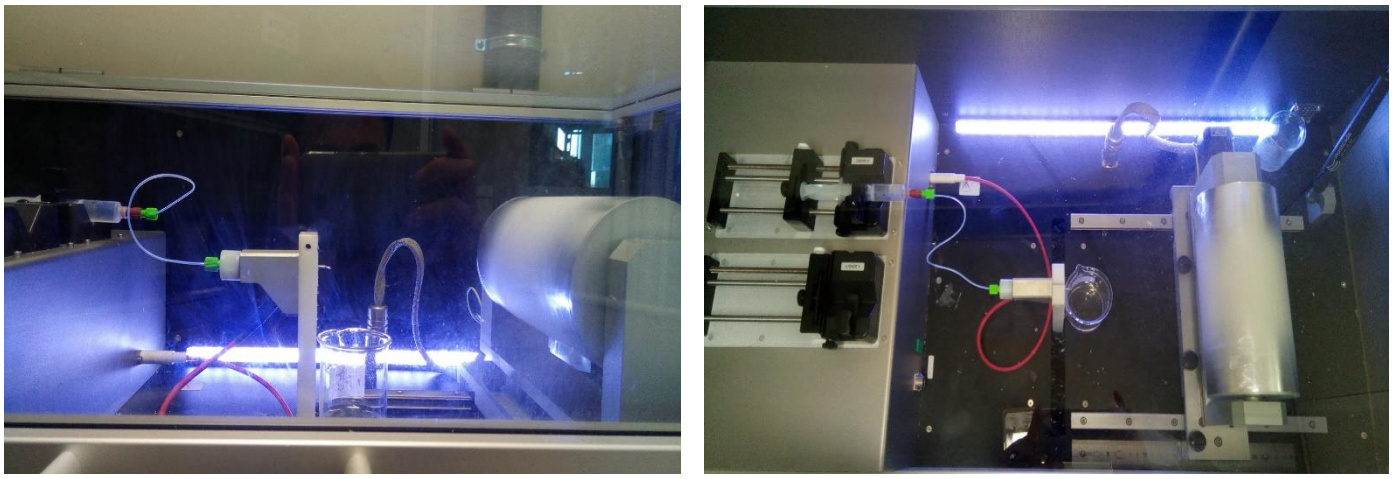

Fig 10 - Electrospinning apparatus used

Figure 10 shows the apparatus used for the electrospinning technique, were the polymer solution is place inside a syringe that is connected to a needle located at a fixed distance from the collector. The polymer solution is pumped through the needle tip and an applied electric field causes the evaporation of the solvent, resulting in the deposition of fibres in the collector.

To produce the membranes, PU pellets were dissolved in dimethylformamide and tetrahydrofuran (1:1), until complete dissolution. The ZnO precipitated powder was then added to the polymer solution, under constant stirring. For this experiment, it was used the ZnO powder with the higher specific surface area (nZnO1)

To produce the 10, 25, and 50% PU/ZnO composites, 1 g of PU was dissolved in a 10 ml mixture of DMF and THF (1:1). Then, different quantities of ZnO powder were added to the solution, in order to attain the desired concentration, and were left under constant stirring overnight. The amounts of the several reagents necessary to the preparation of the different types of PU/ZnO composites are presented in Table 8. The final solutions

were electrospun using a flow rate of 0.5 mL/h, with the distance between the tip of the needle and the collector of 17cm, and with a voltage of 15kV.

The 0% membrane (pure PU) was produced by adding 1 g of PU to 10 ml solution composed of DMF and THF (1:1), left under constant stirring overnight, and electrospun using the same conditions as previously mentioned.

Table 8 - Quantities of the precursors used in the preparation of the various composites.

ZnO amount on the PU/ZnO composites	DMF (ml)	THF (ml)	PU (g)	ZnO (g)
0%	5	5	1	0.00
10%				0.10
25%				0.25
50%				0.50

Fig 12 summarizes the main steps followed in the preparation of the PU and PU/ZnO composite membranes.

Keeping in mind the vascular application of the membranes to produce in the present work it was important that the average fiber diameter was identical to the ECM fibers diameter [4]. For that, several electrospinning conditions were tested.

The electrospun solution was composed of 1g of PU dissolved in 10 mL of a mixture of DMF and THF (1:1). The tested conditions were as resumed in Table 9.

Table 9: Tested parameters for the different set of conditions

Conditions	Voltage (kV)	Flow rate (mL/h)	Distance from collector (cm)
1	15	0,5	**17**
2	15	0,5	**15**
3	15	1,0	**15**
4	15	1,0	**17**

The fiber diameter, calculated using Imagej software, comparisons is presented in the Fig 11.

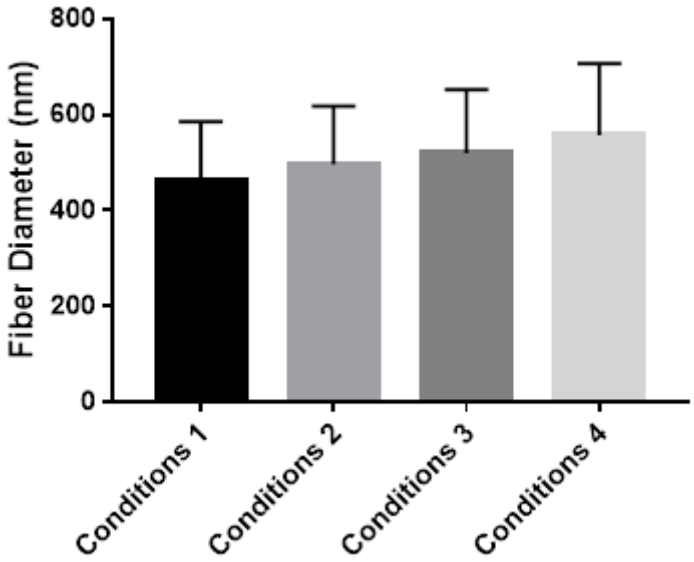

Fig 11 - Fiber diameter variations for the different parameters used

Through the analysis of the fibre diameter, one can conclude that the most suitable set of conditions is the one used in Conditions 1, as the average fiber diameter is in the range of those presented in the ECM [4]. Based on this data these were the chosen conditions.

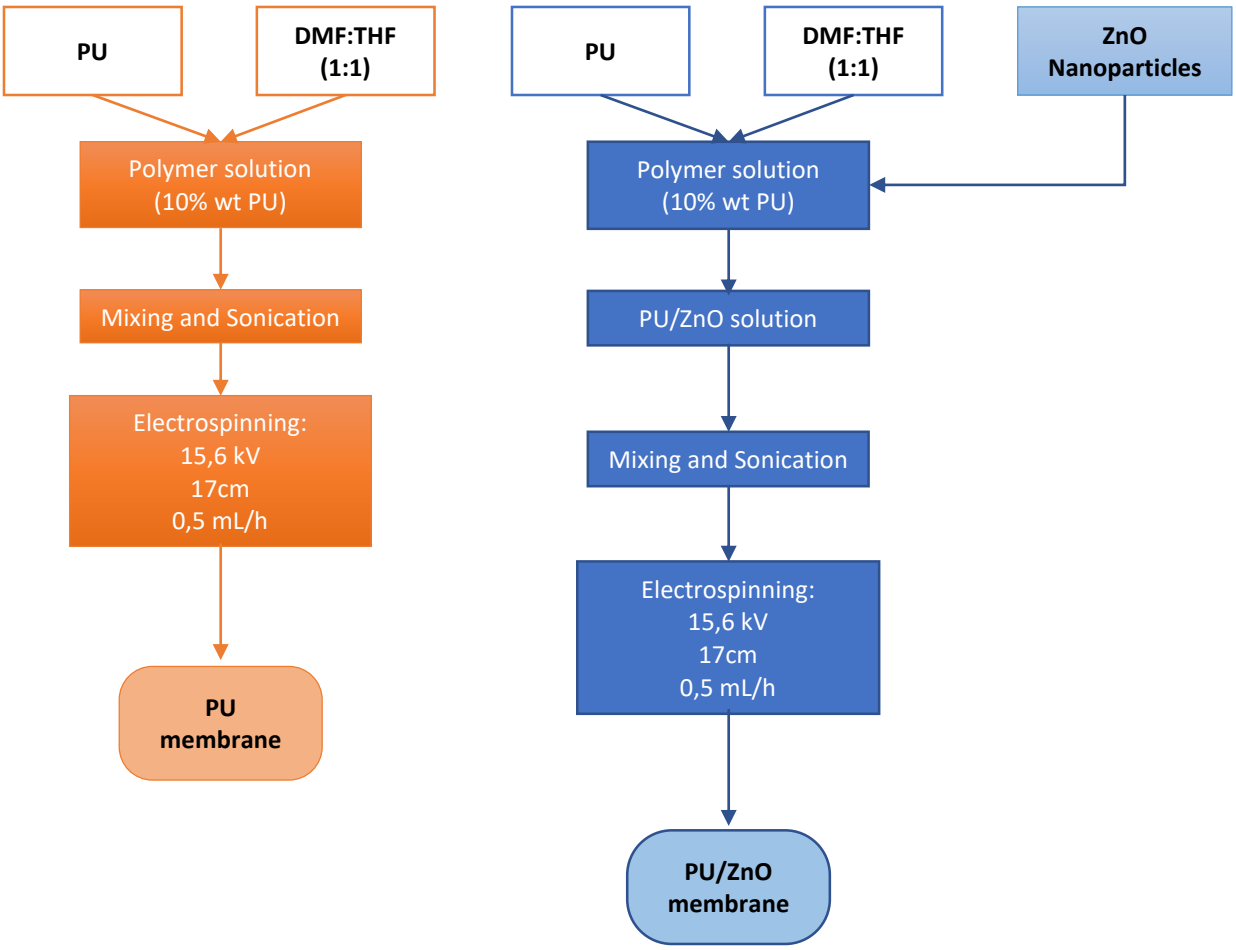

Fig 12 - Flowchart of the production of pure PU and composite membranes

3.4. Anti-bacterial assays

The antibacterial essays were carried out according to the ASTM E2149 method, with respective modifications, named ‘’Determination of the Antibacterial activity of Antibacterial Agents immobilized under conditions of dynamic contact’’ [54].

This is a sensitive method, and commonly used to measure the antibacterial activity of irregular or hydrophobic surfaces.

The assays were carried out using the bacteria Escherichia Coli and Staphylococcus Aureus, due to the fact that both are well known and both are normally recommended as models for this type of tests [55].

The procedure has a duration of 3 days and can be summarized in the following main steps: incubation of the bacterial culture, at 37ºC during at least 16h, addition of the bacterial suspension to a phosphate based buffer and, insertion of the PU or composite membranes to the buffer solution, followed by incubation under constant stirring for 1h;

decimal dilutions of the incubated suspensions; superficial seeding on petri plaques; incubation during 16-24h at 37ºC and finally counting of the Colony Forming Unities (CFU).

The tests with the PU/ZnO membranes, were started placing 1 sample (12 mm diameter each) of pure PU membrane and the membrane containing 50% ZnO content in 1mL of bacterial suspension. This was made in order to establish a baseline. The concentration was gradually increased to 3 and then 5 samples (12 mm each) of each membrane. These concentrations were selected because in the membranes, the zinc oxide particles are dispersed in a polyurethane matrix which can attenuate the effects of the zinc oxide.

The detailed procedure of the essays for the determination of bacterial viability can be consulted in the Annexes.

3.5. Characterization Techniques

3.5.1. X-ray Diffraction (XRD) analysis

XRD analysis is a powerful nondestructive technique that allows the identification of the crystalline phases of the material, such as lattice parameters, crystallite size and crystallographic orientation [56], [57]. This technique is based on the interaction of x-rays with the target surface and its diffraction into many specific direction. According to Bragg's law (Fig 13), only favourably oriented atomic planes relatively to the incident radiation lead to constructive interferences of diffracted radiation [58], [59]:

$$n\lambda = 2d_{hkl}\sin\Theta$$

in which the 'nλ' is the constructive phase difference, 'd_{hkl}' is the interplanar distance and 'Θ' is the reflection angle between a crystallographic plane and the incident radiation with wavelength 'λ' (Fig 13) [56].

Through the variation of the diffraction angle, 2Θ and measuring the intensity of the diffracted beam, which depends of the number of atomic planes evenly spaced, a diffractogram is obtained, which can be compared against a database to help identify the structure of the material [60].

The average crystallite size 'D' is related to the width of a peak in the x-ray in a scan from Θ to 2Θ diffraction and can be calculated using the Debye-Scherrer equation [61]:

$$D = \frac{K\lambda}{\beta \cos \Theta}$$

where λ is the wavelength, Θ is the diffraction angle analysed K is the a factor (it assumes the value of 0.89 for spherical surfaces). β is defined as:

$$\beta = \sqrt{(A_{obs}^2 - a^2)}$$

where A_{obs} refers to the width at half height of the sample peak being analyzed, and a refers to the width at half height of the peak of a standard sample.

X-ray diffraction analysis was used to identify the crystalline phases compositions of the materials studied (precipitates and commercial zinc oxide powders, polyurethane, and PU/ZnO composites) and to calculate crystallite sizes (TC), through the Debye-Scherer equation.

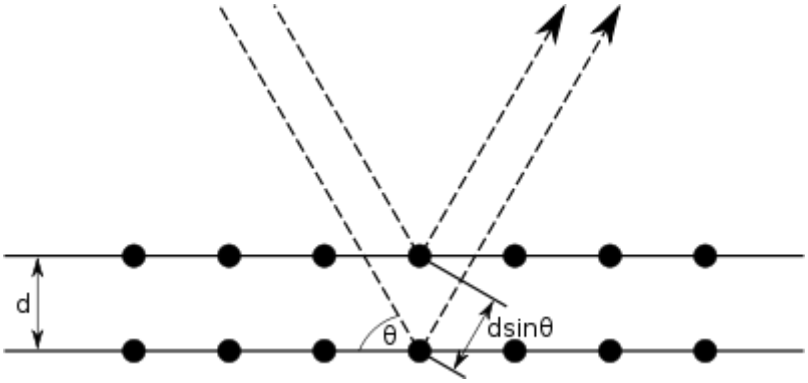

Fig 13 - Visual representation of Bragg's Law

3.5.2. N_2 Isotherm Analysis

An adsorption isotherm curve represents the relation, at constant temperature between the quantity of the gas adsorbed at the surface of the material and the partial pressure at which it occurs. Usually it is represented as a quantity adsorbed in function of the relative pressure (p/p^o), where p and p^o are the pressure and the saturation pressure of the adsorbed substance at the assay temperature, respectively. The adsorption isotherm proposed by Braunauer, Emmet and Teller (BET isotherm) describes the gas adsorption on a material surface in four basic stages [62].

In the first stage the gas molecules adsorb at the material surface through Van der Waals forces. With the rise of pressure, more gas molecules adsorb till a complete monolayer is achieved (stage 2) and with the further increase of pressure new gas layers are formed (stages 3 and 4).

Currently, and accordingly to IUPAC, there are six types of classifications for the gas adsorption isotherms. (Fig 14)

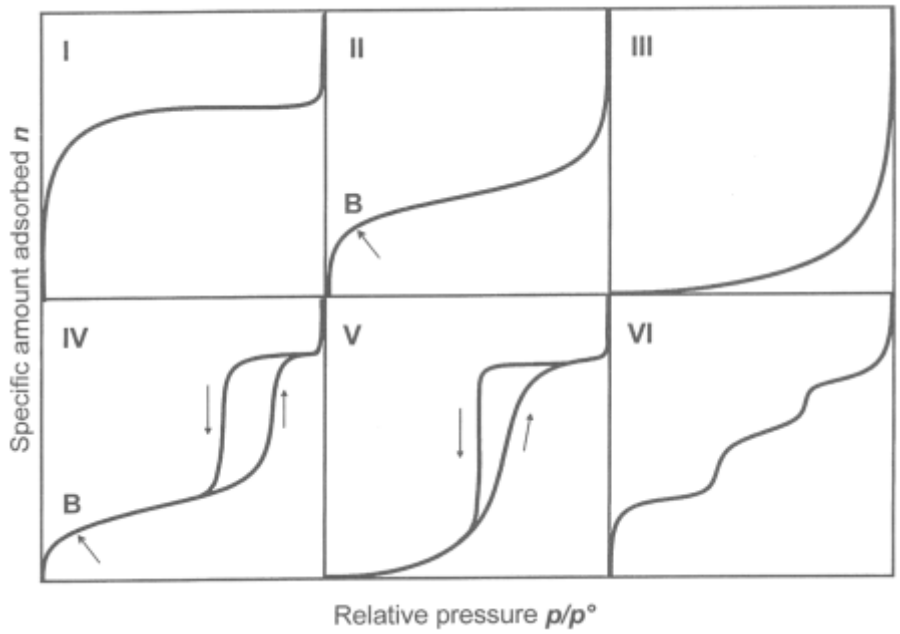

Fig 14 - IUPAC classification for gas adsorption isotherms

Table 10 – Summary of the six types of isotherms

Type I	The Type 1 (also known as Langmuir isotherm) is characteristic of microporous solids with low external surface. It presents a baseline corresponding to the filling of the micropores and its height is related to the porous volume**.**
Type II	It is associated with non-porous materials where point B corresponds to monolayer formation.
Type III	This type of isotherm is not common and is associated with an energy adsorption lower than Type 2.
Type IV	Presented by mesoporous materials.
Type V	It occurs in micro and mesoporous materials, in which the adsorption is based on a weak gas / solid interaction.
Type VI	It is associated with non-porous uniform surfaces and translates a multilayer adsorption mechanism.

The phenomenon of adsorption hysteresis occurs when the adsorption isotherm does not coincide with the desorption isotherm. According to the IUPAC classification, generally, four main hysteresis curves types are considered and are represented Fig 15. Each hysteresis cycle is associated to different pore structures [60].

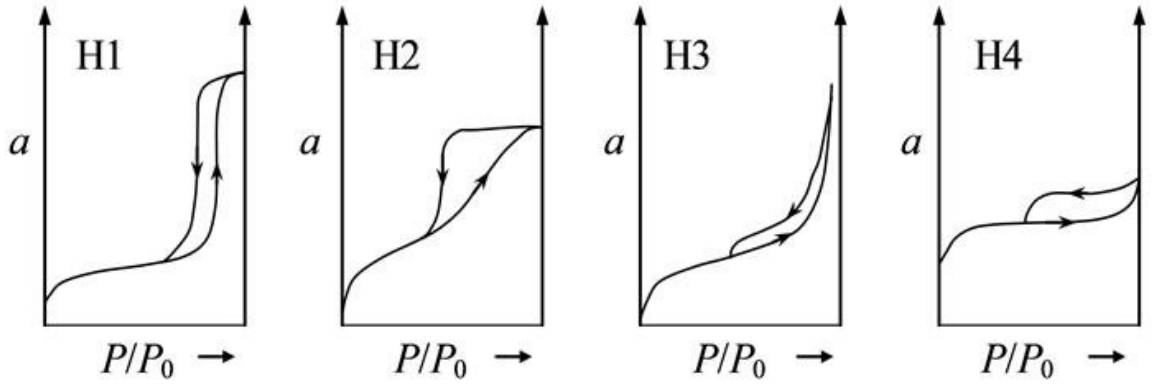

Fig 15 - Classification of hysteresis cycles (irreversible adsorption / desorption processes) according to IUPAC classifications

Table 11 - Summary of different types of hysteresis

H1	Presents two, almost, parallel branches and is associated to porous materials consisting of rigid agglomerates of spherical particles of uniform size.
H2	Presents a vertical desorption branch and is associated to different mechanisms of condensation and evaporation in bottle-shaped pores (narrow neck and broad body).
H3	Associated with aggregates of plate-shaped particles, causing slit pores.
H4	Characterized by two almost horizontal and parallel branches and is associated with narrow slit pores

3.5.3. Brunauer, Emmet and Teller (BET) Model

The BET model, applied to the adsorption isothermals analysis, is used to determine the specific surface area of the nanoparticles [63]. The model assumes a dynamic equilibrium between adsorption and desorption, supposing that the adsorption can occur in multi-layer. The BET equation is used in a linear form [64]:

$$\frac{\frac{p}{p^{\circ}}}{n^{ads}\left(1-\frac{p}{p^{\circ}}\right)} = \frac{1}{n_m^a c} + \frac{c-1}{n_m^a c}\frac{p}{p^{\circ}}$$

where *p* is the pressure at equilibrium, p∘ is the saturation pressure at the adsorption temperature, n^{ads} is the adsorbed quantity at *p* pressure and n_m^a is is the amount adsorbed required to fill the monolayer. The c parameter is called the BET constant is given by:

$$c = e^{(E_1 - E_L)/RT}$$

where E_1 and E_L represent the relative adsorption heat in the first layer and the heat of vapor condensation, respectively [62]. The area that a monolayer occupies at the surface

of the solid may be related to the amount adsorbed on the monolayer by the following expression:

$$ASE = n_m^a N_A a_m$$

where NA corresponds to the number of Avogadro and am is the mean area by one molecule of adsorbate in the monolayer.

The specific surface area of nZnO was thus determined based on the physical adsorption of nitrogen gas, using the isotherm equation of Brunauer, Emmett and Teller (BET).

In this study, a Micrometrics_Gemini 2370V5 equipment was used to measure the specific surface area of the zinc oxide produced powders. The samples were degassed at 100ºC overnight in order to eliminate any gases or vapors adsorbed on the surface of the materials.

3.5.4. Scanning Electron Microscopy (SEM)

The principle of operation of Scanning Electron Microscopy is based on the bombardment of the surface of the material under study with a highly energetic electron beam (usually between 0.1 and 30 keV), resulting in the emission of electrons and photons. The electrons and photons emitted by the material will give rise to the image of the surface topography of the material [59].

Both the powders and the composites were characterized through SEM technique.

The morphology of the composite membranes was observed through SU-70 Hitachi SEM. Samples for SEM can have any format, as long as they are supported by the sample holder. Normally, the samples are covered by a thin film of carbon or gold in order to give them electrical conductivity.

All samples (pure PU membranes and composite membranes) were subjected to deposition of a thin carbon film on Emitech K950 equipment.

In order to observe the samples, a small piece of carbon tape (Neubauer Chemikalien) was glued onto a flat aluminum sample holder. Subsequently, a very small amount of ZnO powder (2 to 3 mg) or composite membrane was placed on the adhesive tape.

The diameters of the electrospun PU-ZnO fibers were, then measured using the micrographs obtained after SEM analysis with the help of ImageJ software.

3.5.5. Energy Dispersive Spectroscopy (EDS)

The technique is commonly used for elemental and compositional analysis of the sample. It is based on the detection of secondary X radiation emitted by the sample as a result of the ionization of its atoms, due to its interactions with the incident electron beam that results in the ejection of electrons from one of the inner orbitals of the atoms (low energy levels) of the sample, leading to the formation of holes. To facilitate the return of the atom to its fundamental energy state, the electrons of the outermost orbitals (higher energy levels) tend to occupy the formed holes. The energy difference between these atomic levels leads to the emission of X radiation, which is collected by a suitable detector (dispersive energy spectrometer) thus allowing the identification and quantification of the constituent elements of the sample [65].

The equipment used for SEM is sufficient to generate the electron beam required for EDS analysis. The X-ray detector used for EDS analysis is therefore normally integrated in SEM systems. The EDS method allows the rapid analysis of individual chemical elements of a sample by comparing the obtained spectrum with known X-ray energy values and element characteristics.

3.5.6. Differential Thermal and Thermogravimetric Analysis (DTA/TG)

The differential thermal analysis (DTA) aims to identify the nature of the reactions that occur during the material heating as well as to identify the temperatures at which the main transformations occur. The thermogravimetric (TG) analysis intends to investigate the mass variation of the material as a function of the temperature variation. In this work, these analyzes were performed on a Seteram Labsys 1600 DTA / TG-DSC equipment. For this purpose 10 mg of ZnO were placed in an alumina crucible and a heating rate of 10 ° C min^{-1} was used. The analysis was carried out with an inert atmosphere of argon.

In the present work, the technique was used to study the thermal behavior of the produced ZnO powders.

3.5.7. Mechanical Assays

The mechanical properties of the PU-ZnO membranes were determined using a Shimadzu MMT-101N (Shimadzu Scientific Instruments, Kyoto, Japan) with a load cell of 100N. The composite membranes were analysed via tensile tests. The tensile properties of the membranes were calculated through the analysis of the stress-strain curves taking into account the slope of the stress – strain curve at low strain (0-5%) Fig 16.

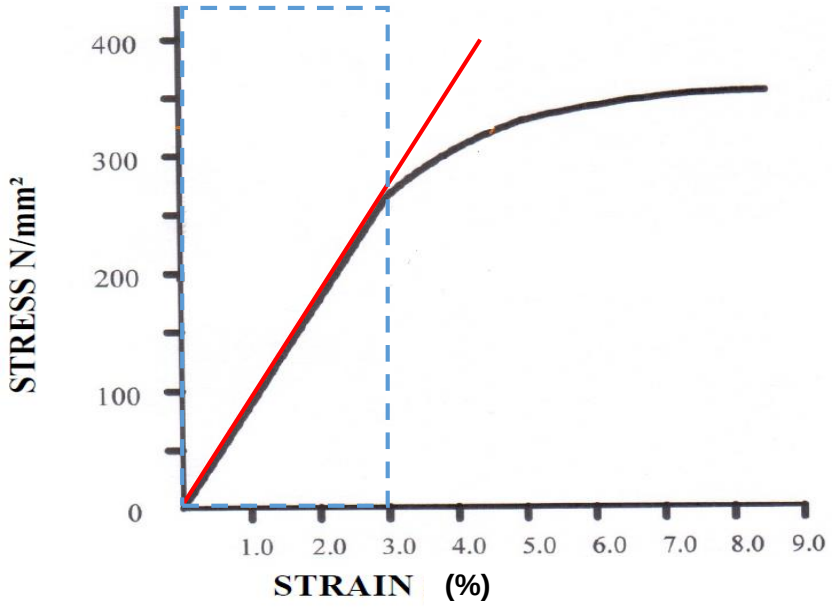

Fig 16 - Graph used for the calculation of the tensile strength value, calculated through the slope of the trend line in the 0-3% range

The essays were performed in triplicate, meaning that three stripes with a 3 cm length and a 1cm width were cut from each membrane sample. The stretched length, corresponding to the L0 was 1 cm. In Fig 17 we can see the schematics of the working apparatus.

Fig 17 - Schematics of the used apparatus for testing the mechanical properties of the membranes

CHAPTER IV

RESULTS AND DISCUSSION

4.1. Zinc Oxide Particles

4.1.1. Crystal phase composition, shape and particle size

The ZnO powders, produced by chemical precipitation were analyzed using XRD, SEM and BET.

Fig 18 shows the X-ray diffractogram (XRD) of the ZnO samples studied in this work. The samples present a single hexagonal phase, with intense peaks, narrow and well defined indicating high crystallinity. According to ZnO crystal data sheet (file JCPDS 04-008-8198) the diffraction peaks were indexed to the Wurtzite type hexagonal unit cell.

Through this we can conclude that it is possible to produce ZnO nanoparticles using a chemical precipitation method, with the occurrence of a single crystalline phase.

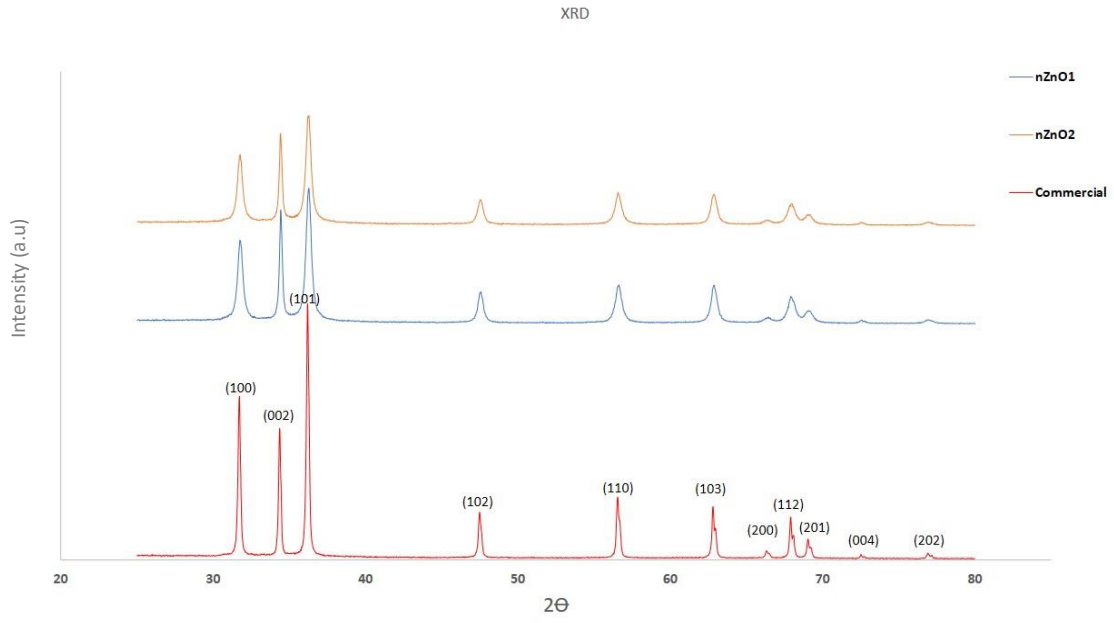

Fig 18 - XRD of the ZnO samples

The intensity ratio of the XRD peaks corresponding to the planes (002) and (101), i.e$\frac{I_{(002)}}{I_{(101)}}$,is 0.46, 0.84 and 0.85 for commercial ZnO, nZnO1 and nZnO2, respectively. As these values are greater than the standard value for wurtzite ZnO (0.44), we can admit the

occurrence of different crystallographic orientations in both the powders produced via chemical precipitation (nZnO1 and nZnO2)- with regard to the commercial ZnO powder [66].

The crystallite sizes were determined by the Debye-Scherrer equation using the diffraction peak corresponding to the plane (101). The attained values were: 27; 23 and 72 nm for nZnO1, nZnO2 and commercial ZnO, respectively. Among the sinthesized powders, nZnO1 is the one presenting better crystallinity as it has a crystallite size larger than nZnO2.

SEM micrographs presented in Fig 19 and Fig 20 allow observing the differences in particle morphology of the ZnO powders under study. Regarding the commercial ZnO powders, large aggregates of ZnO particles with non-uniform morphology are observed, being well evident the large distribution of particle size, as large ZnO particles coexist with finer (nanometric) particles.

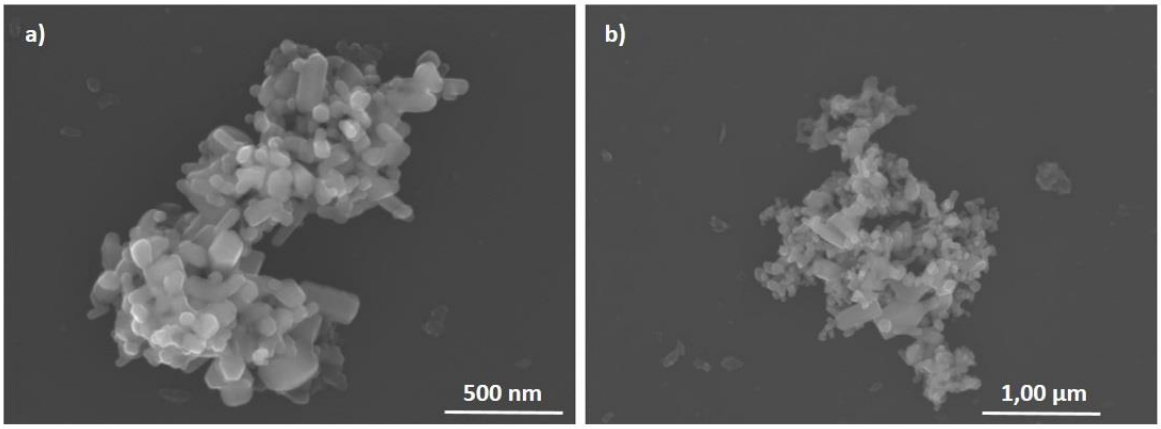

Fig 19 - SEM micrographs of the commercial ZnO powder

Concerning the precipitated powders, they present a spherical urchin-like shape with an organized and complex structure which is composed of assembled ZnO nanoplates possessing an average thickness of 38 and 36 nm for nZnO1 and nZnO2, respectively Fig 20. The measurements were performed on at least 2 micrographs taken in different regions of the sample and more than 30 nanoplates were measured in each micrograph.

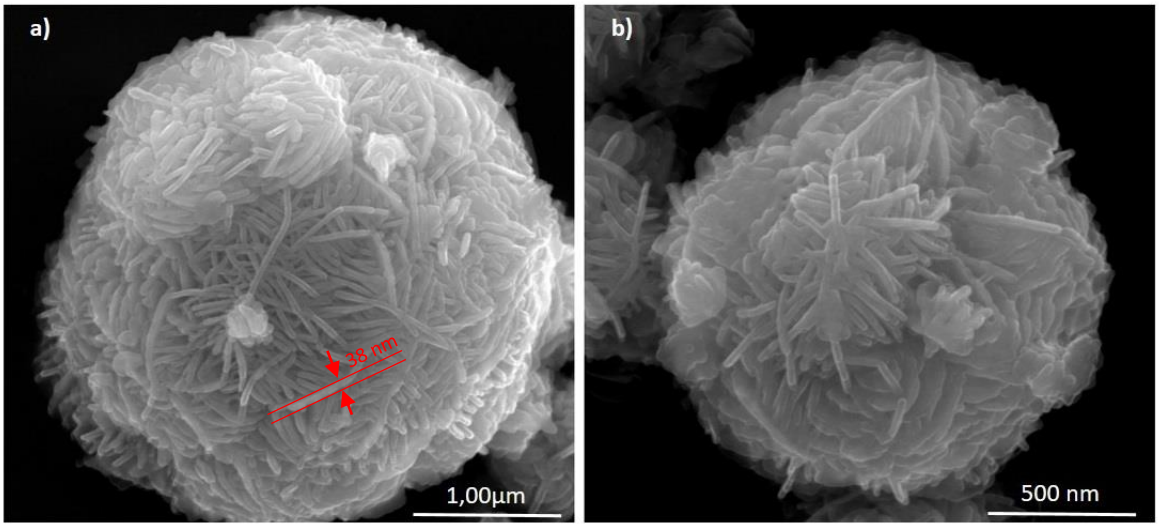

Fig 20 - SEM micrographs of the produced nZnO; a)nZnO1 b)nZnO2

The information regarding the adsorption / desorption isotherms of the ZnO powders and the pore size distribution is presented in Fig 21 and Fig 23

Fig 21 - Adsorption/ Desorption isotherms for different types of ZnO powders: a) commercial; b) nZnO1 and c) nZnO2

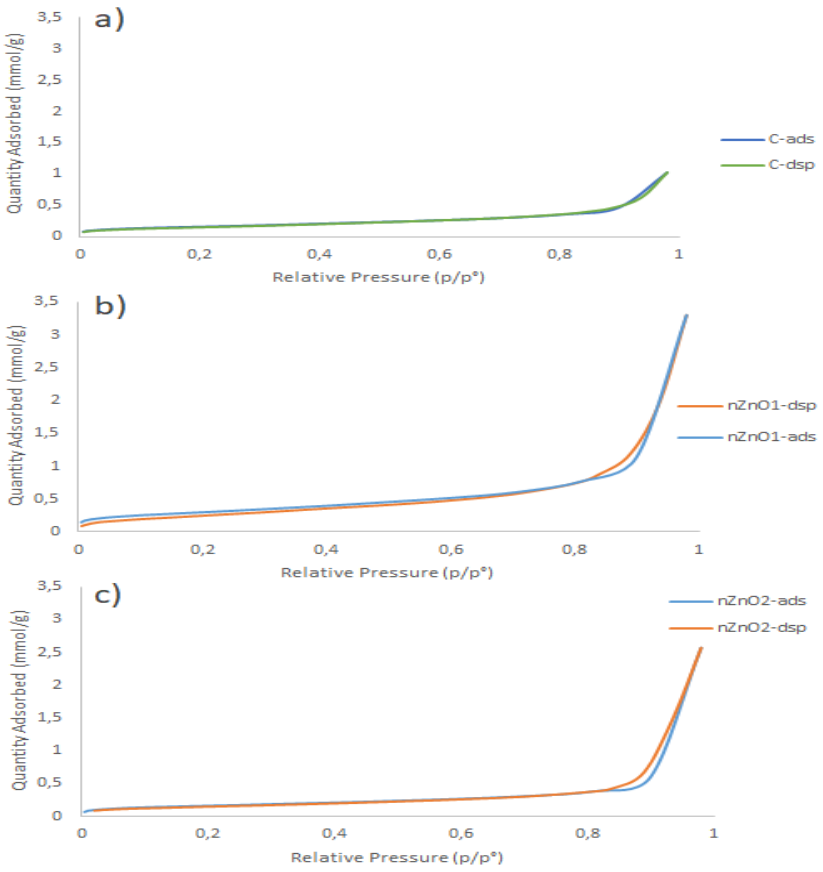

According to IUPAC classification the adsorption/desorption isotherms of the commercial ZnO powder, which do not evidence a hysteric behavior can be classified as type II, typical of non-porous materials.

Regarding the synthesized powders, the obtained curves can be classified as type IV isotherms (UIPAC), typical of mesoporous materials. The shape of the hysteresis curves (type H3 hysteresis) shown in the figure also indicates the presence of slit-like pores. This result is in line with the observations from SEM micrographs of both samples which suggest the presence of slit shape pores between the assembled ZnO nanoplates.

In agreement with the adsorption isotherms (Fig 21), the cumulative pore volume curves (Fig 22) showed differences between the zinc oxide powders: nZnO powders have a total pore volume of approximately $1.2x10^{-1}cm^3/g$, which is substantially higher than the nZnO2 powder, whose total pore volume is approximately $6.0x10^{-2}$.

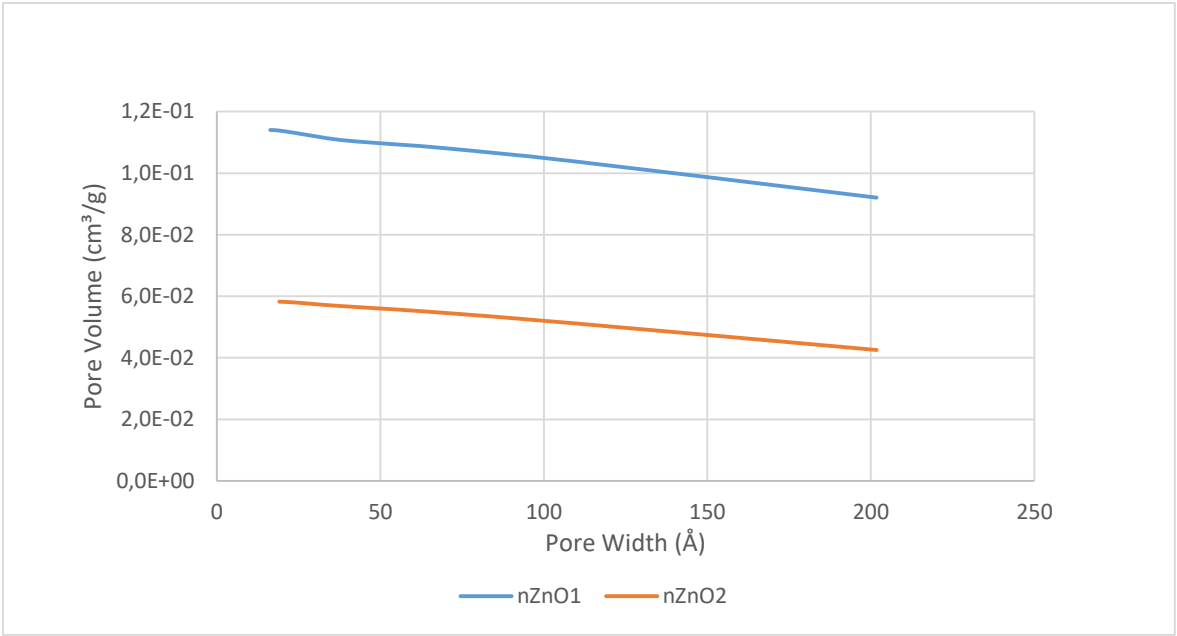

Fig 22: Cumulative pore volume curves of the precipitated powders, nZnO1 and nZnO2

The pore size distribution curves are also significantly different from each other although both powders present bimodal curves. The nZnO1 powder presents a relative maximum pore size of approximately 2.5 nm, high values of dV / dlog(w) can also be observed between 12.5 and 15.0 nm. As for the nZnO2 powder, the highest value of dV / dlog(w) is observed at around 12.5 nm, with an observable peak at 2.5 nm.

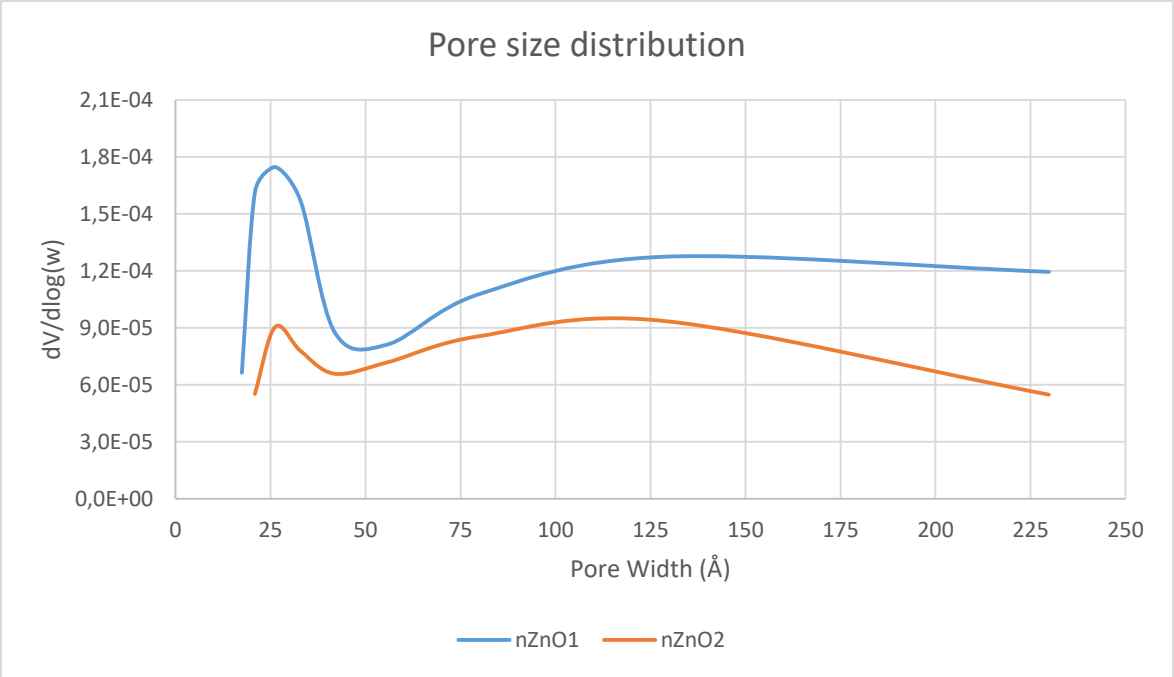

Fig 23 - Pore size distribution curves for the precipitated powders nZnO1 and nZnO2

The specific surface areas (SSA) of nZnO1 and nZnO2 powders are 23.8 m^2/g and 13 m^2/g respectively. It is reported in the literature that zinc oxide nanoparticles synthesized by chemical precipitation presented values of SSA of 21 m^2/g, similar to those obtained for nZnO1 nanoparticles [67]. The pore size distribution curves of the precipitated powders show the importance of fine pores (aprox. 2.5 nm) to the porosity of the particle.

These differences may reflect the processing parameters variation, such as the reagents mixing rate. In the case of nZnO1 the addition rate was of 18 mL/min while for $nZnO_2$ the mixing rate was 13 mL/min. A higher addition rate means that a greater amount of reagent (the basic solution) is added per unit of time to the acidic one. It may be expected that such conditions provide a higher initial supersaturation which could result in a higher nucleation rate, that is, the formation of more nuclei, which would then lead to a larger number of smaller sized particles as compared to the case of $nZnO_2$ [68], [69].

The equivalent spherical diameter (ESD) was determined by [62]:

$$ESD = \frac{6}{SFA \times \rho}$$

where ρ is the theoretical density of ZnO (5,6 g/cm^3)

The values of ESD calculated for nZnO1 and nZnO2 are 45 nm and 82 nm, respectively. These results indicate that although the particles exhibit diameters in the order of microns (exceeding 100 nm which is the size limit normally accepted for “nano” classification), their surface areas are equivalent to particles with a spherical diameter of less than 72 nm, thus supporting the designation of nanoparticles or nanostructured particles.

4.1.2 ZnO Differential Thermal and Thermogravimetric Analysis

The differential thermal analysis of the ZnO nanoparticles (Fig 24) revealed the presence of two endothermic peaks at around 100 and 200 ºC and an exothermic peak right before the 300º C. The peaks seem to be preceded by a loss in mass in the thermogravimetric curve, with the major weight loss occurring at around 250º C. The major weight loss that occurs until the 100ºC mark may be due to the evaporation of water, or the removal of hydroxyl groups in the sample [70], [71]. There is another major weight loss between 220º and 500ºC could be due to the removal and decomposition of organic groups present in the sample during the synthesis. Furthermore there was no significant weight loss above 500º C, indicating that decomposition does not occur above this temperature and that the stable residues may be attributed to ZnO nanoparticles [72]. The high intensity peak at around 300º C is in agreement with the results found in the literature, and is thermal event that can be associated with the a burn-out of organic composition [71], [73], [74].

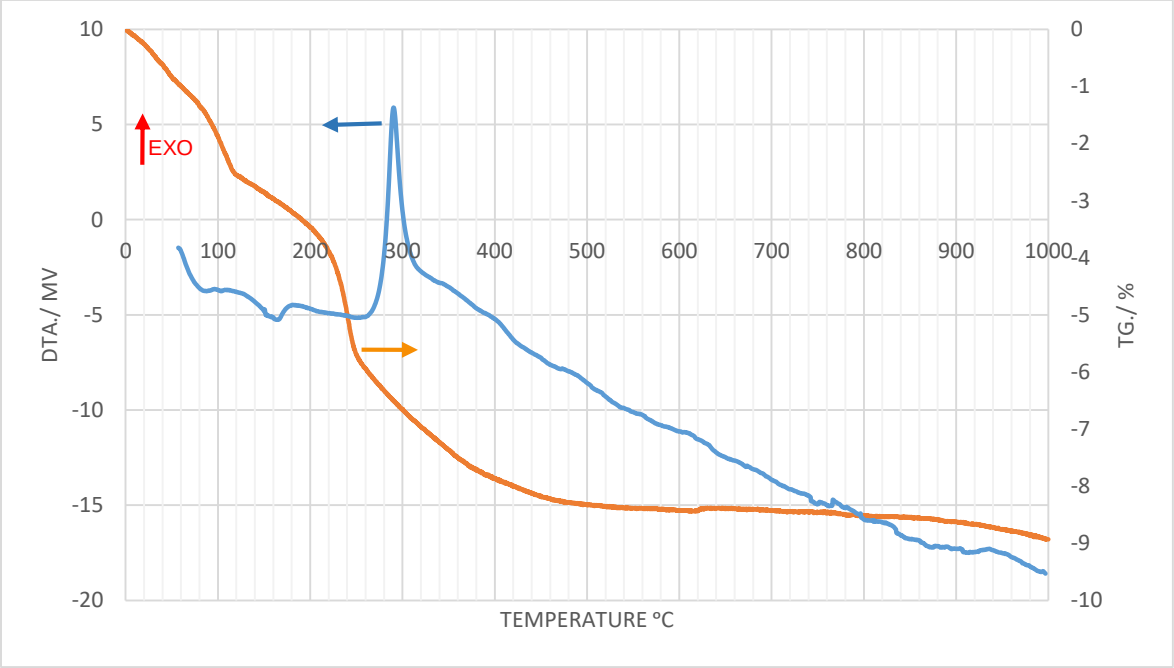

Fig 24 – DTA/TG graph of nZnO1 with a heating rate of 10ºC/min in an Argon atmosphere

As can be seen in Fig 25 the heating of the nanoparticles is accompanied by a structural transformation, resulting from the fusion of the nanoplates due to the heating process which leads to a reduction in SSA.

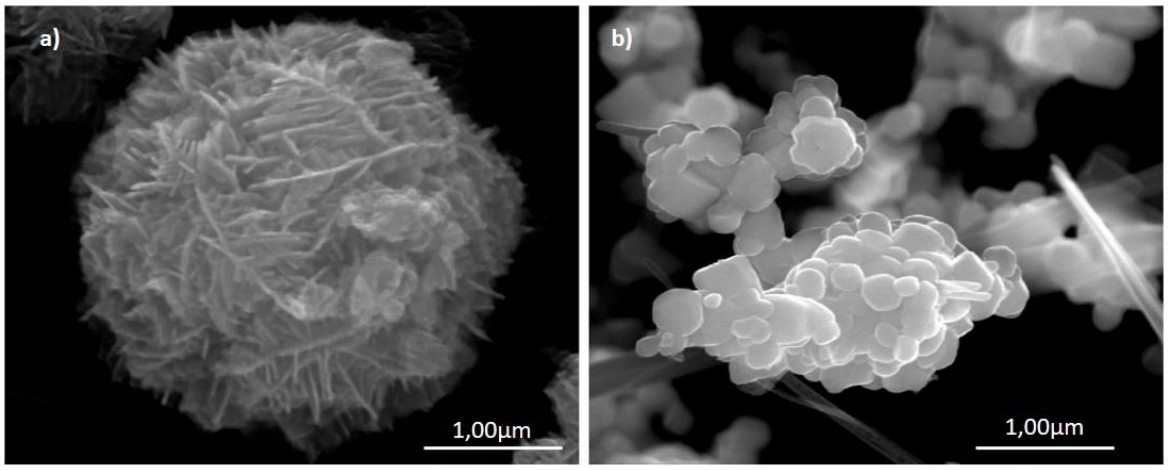

Fig 25 - Structural modifications resulting from the heating process a)nZno1 subjected to 250ºC; b) nZnO1 subjected to 1000º C

4.2. PU/nZnO1 membrane Characterization

As previously mentioned, different membranes were produced with different concentrations of ZnO. The nZnO1 powder was chosen due to its high SSA. The membranes analyzed in this study had a ZnO content of 10, 25 and 50% (zinc oxide mass / total mass of the composite) and were denominated M-10, M-25 and M-50 respectively. The pure PU membrane was denominated M-0.

The membranes were observed by SEM in order to analyze the type of deposition and dispersion of the ZnO nanoparticles. An EDS analysis (Fig 26) was also performed to assess the existence of contaminations. The high intensity peaks shown in the EDS confirm the presence of the ZnO particles in the PU matrix. Some C and Al traces are found in the spectrum coming from the coating and the sample holder. As no other signals were detected within the detection limits of the EDS it can be conclude that the nZnO particles have no contaminations.

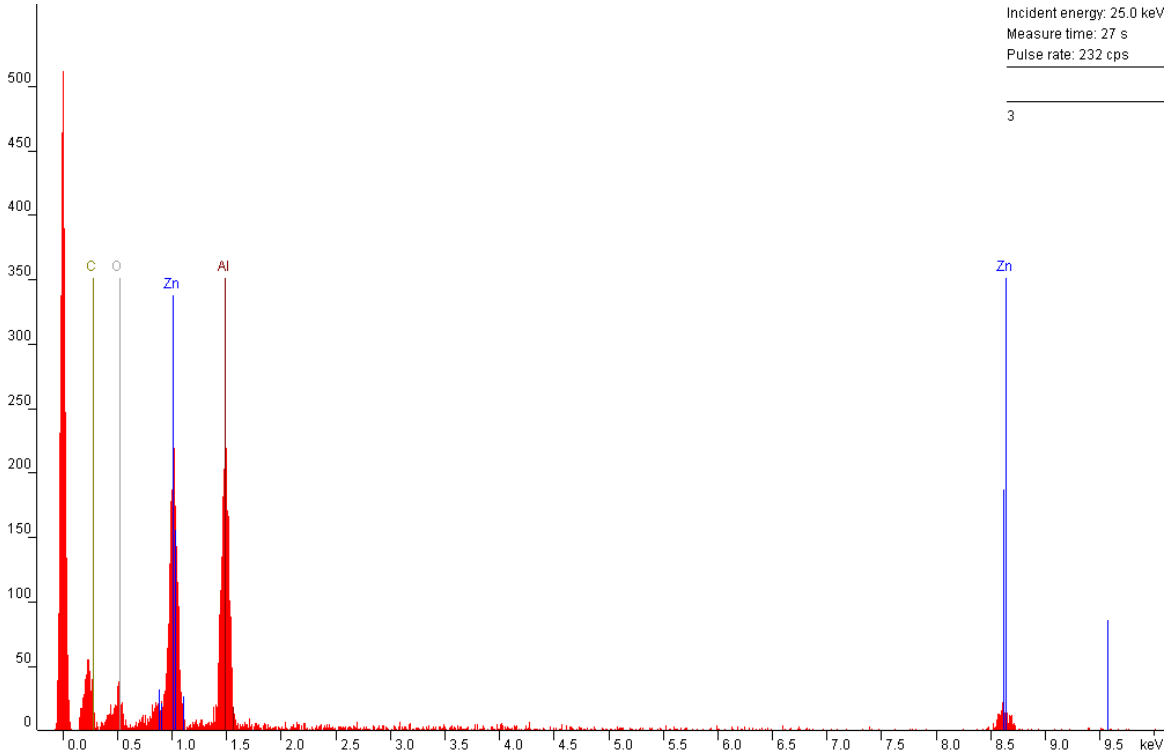

Fig 26 – EDS analysis of the composite membrane

The SEM observations, presented in Fig 27 and Fig 28 show samples of the different composite membranes, as well as a membrane composed of pure PU. The images are ordered from the pure PU membrane (a) to the membrane with the highest content in nZnO (d).The images show the presence of the ZnO nanoparticles in the PU membrane and it is perceptible the increase amount of nanoparticles in the membrane with higher ZnO concentration. The particles appear to be well dispersed throughout the PU matrix. Another important aspect that can be observed in the micrographs is the fact that the ZnO nanoparticles are either embedded in the fibers or entrapped in the matrix.

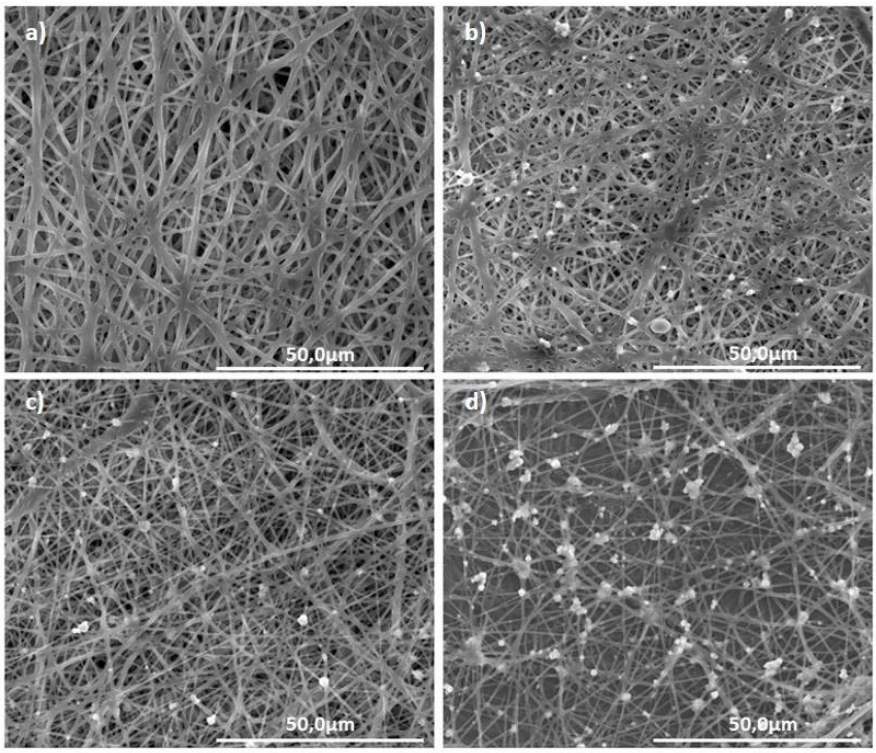

Fig 27 - SEM micrographs of the membranes for different nZnO1 concentrations; a) 0%; b)10%; c)25% and d)50%

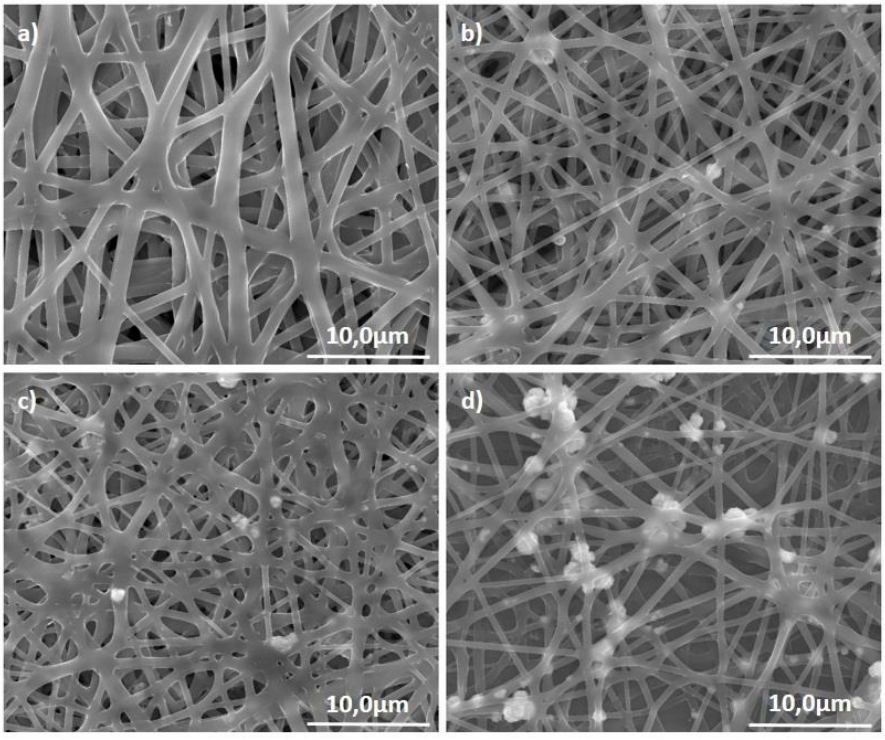

Fig 28 - SEM micrographs of the membranes for different nZnO1 concentrations with higher ampliation ; a) 0%; b)10%; c)25% and d)50%

The thickness of the membranes was also measured, using a micro meter instrument, as it was an important parameter for the tensile strength calculations. The results are presented in Table 12. Previous studies for small diameter blood vessel presented a wall thickness in the ranges of 160 to 930 µm for autologous grafts [75] and 250 µm for PU based grafts, as is the case of Matsuda et. al [29], who worked with commercially available PU and Williamson, who produced PCL-PU composite fibers [76].

When compared to these values the produced PU-nZnO1 composite membranes thickness falls a bit short, this could fixed by increasing the volume of the polymer solution, or further optimization of the electrospinning parameters, because as can be seen for Fig 28 some of the samples (a and c) present fused fibers. Although the electrospinning parameters were the same for all membranes, they have different thickness values, this may be due to external variables such as humidity and temperature, as these play an important role on the conductivity of the polymer solution.

Table 12: Membrane thickness in function of ZnO percentage

ZnO%	Thickness (µm)
0	50
10	110
25	70
50	180

4.3. Antibacterial properties

The antibacterial studies were performed on all membranes, as a way to evaluate the relation of increasing ZnO concentration and its impact on the antibacterial properties of the membrane. The antibacterial properties were tested on both E.coli and S.aureus using the method ASTM-2149 [43].

Antibacterial behavior of PU / nZnO1 membranes

The results from both tests with 1 and 3 disks of each membrane indicated that the concentration of ZnO used was not enough to inflict antibacterial properties. The controller sample used showed more antibacterial activity than the membrane with highest nZnO1 concentration.

As a result the number of disks was increased to 5.

In Fig 29 we can see the results regarding the 5 disk samples for each of the tested concentrations. As can be seen from the data, the results show that the higher the ZnO concentration, the higher the antibacterial activity. The maximum bacterial reduction (70.5%) was achieved for the 50% ZnO concentration.

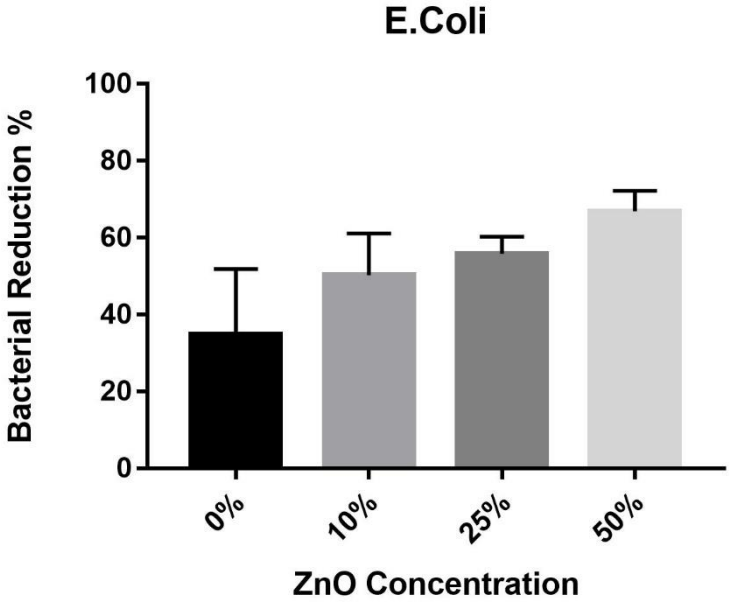

Fig 29 - Bacterial reduction for E.Coli in function of nZnO concentration in PU-nZnO1 composites

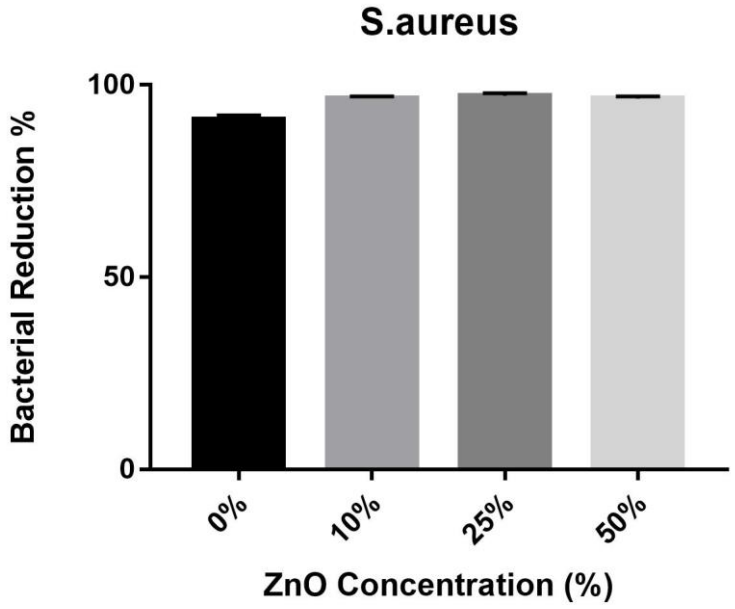

Fig 30 - Bacterial reduction for S.aureus in function of nZnO concentration in PU-nZnO1 composites

The *S.aureus* assay showed an increase in bacterial reduction Fig 30 when compared with the results from the *E.coli*.

For this essay all the parameters were maintained but the used bacterial strain. Once again we can see that bacterial reduction increases with the increase in ZnO concentration. The number of Colony Forming Units (CFU) was significantly reduced with the ZnO filled membranes. There are several mechanisms proposed regarding he antibacterial activity of ZnO nanoparticles, the release of Zn^{2+}ions from the particles; mechanical destruction of the cell membrane caused by the penetrations of nanoparticles; active oxygen from the nanoparticles and the generation of hydrogen peroxide (H_2O_2) from the surface of ZnO [77].

The growth rate of a bacteria can be affected by the interactions with the nanoparticles in the membrane. As the nanoparticles used have a large surface area (23.8 m^2/g) available for interactions, enhancing its antibacterial effect. The ZnO particles may increase the production of active oxygen, such as H_2O_2, and leading to cell death. It is assumed that H_2O_2 generated damages the cell membrane of bacteria, producing some type of injury, and inhibiting the growth of the cells or even killing them. The contact of the nanoparticles with the bacteria may disrupt its respirations, as they interact with the enzymes of the bacteria respiration chains, which in the case of the *E.coli* can account for as much as 87% of the total H_2O_2 production [44].

It is reported in the literature that ZnO nanoparticles may interfere with the pumping activity of NorA protein of S. aureus [78]. The NorA protein mediates the active efflux of hydrophilic fluoroquinolones from the cell, conferring resistance upon the organism. recent reports suggest that nano-sized metal oxides such as zinc oxide and titanium dioxide possess the ability to induce faster electron transfer kinetics in the active site of the enzymes, based on this, it seems likely that ZnO nanoparticles may interfere with the pumping activity of the this protein.

It is also possible that the polymer surfaces slightly degrade during incubation and some ZnO nanoparticles were released into the culture medium where they interfered with bacteria cell membranes.

The difference in activity against these two types of bacteria can be attributed to the structural and chemical compositional differences of the cell surfaces. Gram-positive bacteria typically have one cytoplasmatic membrane and thick wall composed of multilayers of peptidoglycan. However, gram-negative bacteria have more complex cell wall structure, with a layer of peptidoglycan between outer membrane and a cytolasmatic membrane [79]. The antibacterial effect can be attributed to the damage of cell membranes, which leads to leakage of cell contents and cell death. Therefore, the difference in antibacterial action towards *E.coli* and *S. aureus* is assumed to be caused by the different sensitivities towards H_2O_2 generated by the ZnO nanoparticles [77].

4.4. Mechanical Properties of the PU/ZnO membrane

In this work ZnO nanoparticles were introduced in a PU matrix, and thus it becomes important to analyse the effect of nanoparticles in the mechanical properties of the PU based composites.

The results for the tensile strength in function of the ZnO concentration are presented in Fig 31.

It is important to mention that all the samples were stretched to 30% of their original L_0 and no visible signs of rupture were observed or registered.

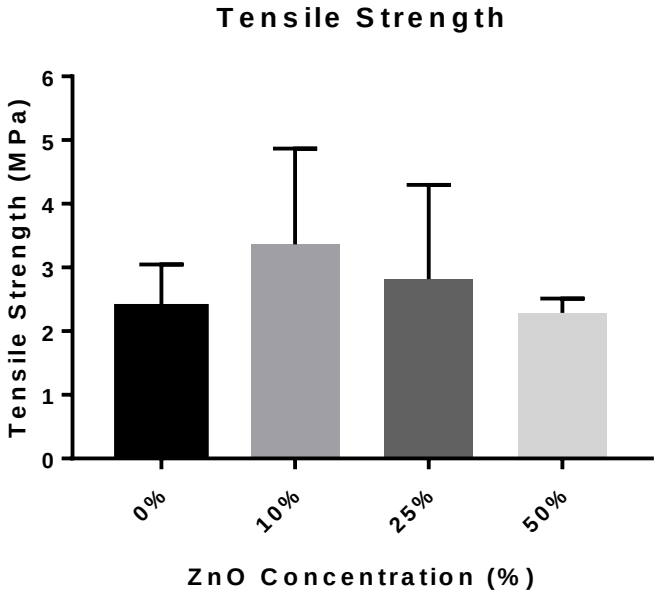

Fig 31 - Tensile strenght value of the membranes in function of the nZnO concentration

The data indicates that the highest tensile strength value was observed for the 10% concentration sample and that the increase of ZnO concentration reduces the tensile strength of the membrane. This may be due to the increase in nanoparticles content causing the increase of defects in the matrix [68].

These results seem to be in agreement with previous studies, although the obtained values are lower. It is important to mention that the previous studies used different nanoparticles structure and a different method for the production of the PU matrix, as Le et. al used commercially available ZnO and his composites were produced via solvent casting [43]. The overall results appear to be better that those of the small blood vessels, as the results from autologous grafts for small diameter blood vessels range from 58 kPa to 2.6 MPa [75], [80].

CHAPTER V

CONCLUSIONS AND FUTURE WORK

CHAPTER V – CONCLUSIONS AND FUTURE WORK

The present work was focused on the development of PU/ZnO composite membranes and its characterization in terms of microstructure, antibacterial and mechanical properties. Zinc oxide presents itself as a polyvalent material, suitable for various applications in the biomedical field, mainly due to its antibacterial properties. However, the mechanisms of the biocidal action of these nanostructures are far from being fully understood.

A suitable way to make use of the zinc oxide antibacterial properties is by enveloping the nanoparticles in a polymer matrix, such as polyurethane.

For this purpose, zinc oxide nanoparticles were synthesized by a method of chemical precipitation. Through the controlled variation of some experimental procedures (Cit:Zn ratio and addition rate) several nanostructured particles were obtained, presenting different characteristics, such as the specific surface area (23.8 m^2/g for nZnO1 and 13 m^2/g for nZnO2). Both samples resulted from the agglomeration of nanometer-sized plates (nZnO1 presented plates with a mean thickness of 38 nm and nZnO2 presented plates with a mean thickness of 36 nm).

Polyurethane composites with nZnO1 as a filler were also produced with zinc oxide contents of 10, 25 and 50% (zinc oxide mass/ PU mass) as well as a pure PU membrane.

The studies of the antibacterial properties were performed against E.coli and S.aureus, and allowed to evaluate the antibacterial activity of the PU/nZnO1 composites for the different concentrations. It was concluded that the antibacterial properties of the composites is dependent on the ZnO content, the higher the content, the higher the observed bacterial reduction.

The mechanical properties of the membranes were also tested and it was concluded that the tensile strength of the composites was increased, when compared to the pure PU membrane. The optimal content of nZnO1 was found to be 10%, as this was the value the presented the highest tensile strength. It was relevant the fact that none of the membranes has suffered any rupture during the assays.

Future Work

The results obtained in the present work require the deepening of certain aspects in order to clarify some data. In this way it is suggested:

- Use a higher volume of the polymer solution as a way to produce thicker membranes, and evaluate their overall behaviour;
- Further optimization of the electrospinning conditions;
- Quantify the reactive oxygen species produced by the ZnO nanoparticles as a way to better understand the antibacterial behaviour of the composite membranes;
- Loading the composite membrane with a drug and trying to establish a controlled release.

BIBLIOGRAPHY

[1] D. G. Seifu, A. Purnama, K. Mequanint, and D. Mantovani, “Small-diameter vascular tissue engineering,” *Nature Reviews Cardiology*, vol. 10, no. 7. pp. 410–421, 2013.

[2] M. Nichols *et al.*, *European cardiovascular disease statistics 2012*. 2012.

[3] G. R. Campbell and J. H. Campbell, “Development of tissue engineered vascular grafts.,” *Curr. Pharm. Biotechnol.*, vol. 8, pp. 43–50, 2007.

[4] D. Massai *et al.*, “Bioreactors as Engineering Support to Treat Cardiac Muscle and Vascular Disease,” *J. Healthc. Eng.*, vol. 4, no. 3, pp. 329–370, 2013.

[5] L. L. Chiu and M. Radisic, “Cardiac tissue engineering,” *Curr. Opin. Chem. Eng.*, vol. 2, no. 1, pp. 41–52, 2013.

[6] D. Suarez Bagnasco *et al.*, “Elasticity assessment of electrospun nanofibrous vascular grafts: A comparison with femoral ovine arteries,” *Mater. Sci. Eng. C*, vol. 45, pp. 446–454, 2014.

[7] R. E. McMahon *et al.*, “Hydrogel–Electrospun Mesh Composites for Coronary Artery Bypass Grafts,” *Tissue Eng. Part C Methods*, vol. 17, no. 4, pp. 451–461, 2011.

[8] L. Gui *et al.*, “Construction of Tissue-Engineered Small-Diameter Vascular Grafts in Fibrin Scaffolds in 30 Days,” *Tissue Eng. Part A*, vol. 20, no. 9–10, pp. 1499–1507, 2014.

[9] P. Punnakitikashem, D. Truong, J. U. Menon, K. T. Nguyen, and Y. Hong, “Electrospun biodegradable elastic polyurethane scaffolds with dipyridamole release for small diameter vascular grafts,” *Acta Biomater.*, vol. 10, no. 11, pp. 4618–4628, 2014.

[10] R. Y. Kannan, H. J. Salacinski, P. E. Butler, G. Hamilton, and A. M. Seifalian, “Current status of prosthetic bypass grafts: A review,” *Journal of Biomedical Materials Research - Part B Applied Biomaterials*, vol. 74, no. 1. pp. 570–581, 2005.

[11] C. V. C. Bouten, P. Y. W. Dankers, A. Driessen-Mol, S. Pedron, A. M. A. Brizard, and F. P. T. Baaijens, “Substrates for cardiovascular tissue engineering,” *Adv. Drug Deliv. Rev.*, vol. 63, no. 4, pp. 221–241, 2011.

[12] B. Dhandayuthapani, Y. Yoshida, T. Maekawa, and D. S. Kumar, “Polymeric scaffolds in tissue engineering application: A review,” *International Journal of Polymer Science*, vol. 2011. 2011.

[13] S. Tara *et al.*, “Vessel Bioengineering,” *Circ. J.*, vol. 78, no. 1, pp. 12–19, 2014.

[14] S. A. Sell, P. S. Wolfe, K. Garg, J. M. McCool, I. A. Rodriguez, and G. L. Bowlin, “The use of natural polymers in tissue engineering: A focus on electrospun extracellular matrix analogues,” *Polymers*, vol. 2, no. 4. pp. 522–553, 2010.

[15] A. Rachev, “Design and Fabrication of a Mechanically Matched Vascular Graft,” *J. Biomech. Eng.*, vol. 133, no. 9, p. 91004, 2011.

[16] A. J. Coury, P. C. Slaikeu, P. T. Cahalan, K. B. Stokes, and C. M. Hobot, “Factors and interactions affecting the performance of polyurethane elastomers in medical devices.”

[17] Q. Chen, S. Liang, and G. A. Thouas, “Elastomeric biomaterials for tissue engineering,” *Prog. Polym. Sci.*, vol. 38, no. 3–4, pp. 584–671, 2013.

[18] X. Zhang, K. G. Battiston, J. E. McBane, L. A. Matheson, R. S. Labow, and J. Paul Santerre, “Design of Biodegradable Polyurethanes and the Interactions of the Polymers and Their Degradation By-Products Within in Vitro and in Vivo Environments,” in *Advances in Polyurethane Biomaterials*, 2016, pp. 75–114.

[19] P. Vermette, H. Griesser, G. Laroche, and R. Guidoin, *Biomedical applications of polyurethanes*. 2001.

[20] J. M. Anderson *et al.*, “Recent Advances in Biomedical Polyurethane Biostability and Biodegradation,” *Polym. Int.*, vol. 46, no. 3, pp. 163–171, 1998.

[21] T. A. Speckhard, K. K. S. Hwang, S. L. Cooper, V. S. C. Chang, and J. P. Kennedy, “Properties of polyisobutylene polyurethane block copolymers: 3. Hard segments based on 4,4′-dicyclohexylmethane diisocyanate (H12MDI) and butane diol,” *Polymer (Guildf).*, vol. 26, no. 1, pp. 70–78, 1985.

[22] T. K. Chen, T. S. Shieh, and J. Y. Chui, “Studies on the first DSC endotherm of polyurethane hard segment based on 4,4′-diphenylmethane diisocyanate and 1,4-butanediol,” *Macromolecules*, vol. 31, no. 4, pp. 1312–1320, 1998.

[23] B. K. Kendagannaswamy and Siddaramaiah, “Chain-extended polyurethanes - Synthesis and characterization,” *J. Appl. Polym. Sci.*, vol. 84, no. 2, pp. 359–369, 2002.

[24] M. Desai, A. M. Seifalian, and G. Hamilton, “Role of prosthetic conduits in coronary artery bypass grafting,” *European Journal of Cardio-thoracic Surgery*, vol. 40, no. 2. pp. 394–398, 2011.

[25] J. W. Boretos and W. S. Pierce, “Segmented polyurethane: A polyether polymer. An initial evalution for biomedical applications,” *J. Biomed. Mater. Res.*, vol. 2, no. 1, pp. 121–130, 1968.

[26] M. F. Maitz, “Applications of synthetic polymers in clinical medicine,” *Biosurface and Biotribology*, vol. 1, no. 3, pp. 161–176, 2015.

[27] P. Uttayarat *et al.*, “Micropatterning of three-dimensional electrospun polyurethane vascular grafts,” *Acta Biomater.*, vol. 6, no. 11, pp. 4229–4237, 2010.

[28] P. H. Blit, K. G. Battiston, M. Yang, J. Paul Santerre, and K. A. Woodhouse, “Electrospun elastin-like polypeptide enriched polyurethanes and their interactions with vascular smooth muscle cells,” *Acta Biomater.*, vol. 8, no. 7, pp. 2493–2503, 2012.

[29] T. Matsuda, M. Ihara, H. Inoguchi, I. K. Kwon, K. Takamizawa, and S. Kidoaki, “Mechano-active scaffold design of small-diameter artificial graft made of electrospun segmented polyurethane fabrics,” *J. Biomed. Mater. Res. - Part A*, vol. 73, no. 1, pp. 125–131, 2005.

[30] R. M. Nezarati, M. B. Eifert, D. K. Dempsey, and E. Cosgriff-Hernandez, “Electrospun vascular grafts with improved compliance matching to native vessels,” *J. Biomed. Mater. Res. - Part B Appl. Biomater.*, vol. 103, no. 2, pp. 313–323, 2015.

[31] D. Cozzens, X. Wei, and R. Faust, “Electrospinning of biostable polyisobutylene-based thermoplastic polyurethanes,” *J. Polym. Sci. Part B Polym. Phys.*, vol. 51, no. 6, pp. 452–459, 2013.

[32] J. Han *et al.*, “Electrospinning and biocompatibility evaluation of biodegradable polyurethanes based on L -lysine diisocyanate and L -lysine chain extender,” *J. Biomed. Mater. Res. - Part A*, vol. 96 A, no. 4, pp. 705–714, 2011.

[33] J. Han, S. Farah, A. J. Domb, and P. I. Lelkes, “Electrospun Rapamycin-Eluting Polyurethane Fibers for Vascular Grafts,” *Pharm. Res.*, vol. 30, no. 7, pp. 1735–1748, 2013.

[34] C. Grasl, H. Bergmeister, M. Stoiber, H. Schima, and G. Weigel, “Electrospun polyurethane vascular grafts: In vitro mechanical behavior and endothelial adhesion molecule expression,” *J. Biomed. Mater. Res. - Part A*, vol. 93, no. 2, pp. 716–723, 2010.

[35] M. W. Radomski, R. M. Palmer, and S. Moncada, “The role of nitric oxide and cGMP in platelet adhesion to vascular endothelium.,” *Biochem. Biophys. Res. Commun.*, vol. 148, no. 3, pp. 1482–9, 1987.

[36] C. F. Klingshirn, “ZnO: Material, physics and applications,” *ChemPhysChem*, vol. 8, no. 6. pp. 782–803, 2007.

[37] Z. L. Wang, “Zinc oxide nanostructures: growth, properties and applications,” *J. Phys. Condens. Matter*, vol. 16, pp. R829–R858, 2004.

[38] W. H. De Jong and P. J. A. Borm, “Drug delivery and nanoparticles: Applications and hazards,” *International Journal of Nanomedicine*, vol. 3, no. 2. pp. 133–149, 2008.

[39] S. Xu and Z. L. Wang, “One-dimensional ZnO nanostructures: Solution growth and functional properties,” *Nano Research*, vol. 4, no. 11. pp. 1013–1098, 2011.

[40] C. Chen, P. Liu, and C. Lu, “Synthesis and characterization of nano-sized ZnO powders by direct precipitation method,” *Chem. Eng. J.*, vol. 144, no. 3, pp. 509–513, 2008.

[41] J. You, Y. Zhang, and Z. Hu, “Bacteria and bacteriophage inactivation by silver and zinc oxide nanoparticles,” *Colloids Surfaces B Biointerfaces*, vol. 85, no. 2, pp. 161–167, 2011.

[42] L. Zhang, Y. Jiang, Y. Ding, M. Povey, and D. York, “Investigation into the antibacterial behaviour of suspensions of ZnO nanoparticles (ZnO nanofluids),” *J. Nanoparticle Res.*, vol. 9, no. 3, pp. 479–489, 2007.

[43] J. H. Li, R. Y. Hong, M. Y. Li, H. Z. Li, Y. Zheng, and J. Ding, “Effects of ZnO nanoparticles on the mechanical and antibacterial properties of polyurethane coatings,” *Prog. Org. Coatings*, vol. 64, no. 4, pp. 504–509, 2009.

[44] N. Jones, B. Ray, K. T. Ranjit, and A. C. Manna, “Antibacterial activity of ZnO nanoparticle suspensions on a broad spectrum of microorganisms,” *FEMS Microbiol. Lett.*, vol. 279, no. 1, pp. 71–76, 2008.

[45] G. Appierot *et al.*, “Enhanced antibacterial actiwity of nanocrystalline ZnO due to increased ROS-mediated cell injury,” *Adv. Funct. Mater.*, vol. 19, no. 6, pp. 842–852, 2009.

[46] A. Sirelkhatim *et al.*, “Review on zinc oxide nanoparticles: Antibacterial activity and toxicity mechanism,” *Nano-Micro Letters*, vol. 7, no. 3. pp. 219–242, 2015.

[47] K. R. Raghupathi, R. T. Koodali, and A. C. Manna, “Size-dependent bacterial growth inhibition and mechanism of antibacterial activity of zinc oxide nanoparticles.,” *Langmuir*, vol. 27, no. 7, pp. 4020–4028, 2011.

[48] D. P. Jones, “Redox potential of GSH/GSSG couple: Assay and biological significance,” *Methods Enzymol.*, vol. 348, pp. 93–112, 2002.

[49] R. Vasita and D. S. Katti, “Nanofibers and their applications in tissue engineering,” *International Journal of Nanomedicine*, vol. 1, no. 1. pp. 15–30, 2006.

[50] C. H. Bludworth Joseph E, “Apparatus for producing artificial filaments from material such as cellulose acetate,” US2482834, 1934.

[51] Y. Hong, “Electrospun Fibrous Polyurethane Scaffolds in Tissue Engineering,” in

Advances in Polyurethane Biomaterials, 2016, pp. 543–559.

[52] D. N. Rockwood, R. E. Akins, I. C. Parrag, K. A. Woodhouse, and J. F. Rabolt, “Culture on electrospun polyurethane scaffolds decreases atrial natriuretic peptide expression by cardiomyocytes in vitro,” *Biomaterials*, vol. 29, no. 36, pp. 4783–4791, 2008.

[53] J. L. Luís, “Compósitos de PU/ZnO para aplicações biomédicas,” Aveiro University, 2011.

[54] ASTM International, “ASTM E2149: Standard Test Method for Determining the Antimicrobial Activity of Immobilized Antimicrobial Agents Under Dynamic Contact Conditions 1,” vol. West Consh, p. Pennsylvania, 2013.

[55] M. Chen, Z. Yang, H. Wu, X. Pan, X. Xie, and C. Wu, “Antimicrobial activity and the mechanism of silver nanoparticle thermosensitive gel.,” *Int. J. Nanomedicine*, vol. 6, pp. 2873–2877, 2011.

[56] L. Pereira, “Produção e caracterização de silício policristalino e sua aplicação a TFTs,” *Mater. Ing.*, vol. PhD Tesis, 2008.

[57] B. D. Cullity and S. R. Stock, *Elements of X-ray diffraction, 3rd edition*. 2001.

[58] S. Bandyopadhyay, J. R. Peralta-Videa, J. A. Hernandez-Viezcas, M. O. Montes, A. A. Keller, and J. L. Gardea-Torresdey, “Microscopic and spectroscopic methods applied to the measurements of nanoparticles in the environment,” *Applied Spectroscopy Reviews*, vol. 47, no. 3. pp. 180–206, 2012.

[59] Y. Leng, *Materials characterization: Introduction to microscopic and spectroscopic methods: Second edition*. 2013.

[60] P. Atkin and J. Paula, *Physical chemistry*. 2006.

[61] A. L. Patterson, “The scherrer formula for X-ray particle size determination,” *Phys. Rev.*, vol. 56, no. 10, pp. 978–982, 1939.

[62] P. M. Donohue, “Adsorption Isotherms with Hysteresis Loops,” *Pure Appl. Chem.*, 1985.

[63] S. Brunauer, P. H. Emmett, and E. Teller, “Adsorption of Gases in Multimolecular Layers,” *J. Am. Chem. Soc.*, vol. 60, no. 2, pp. 309–319, 1938.

[64] J. Rouquerol, F. Rouquerol, P. Llewellyn, G. Maurin, and K. S. W. Sing, *Adsorption by Powders and Porous Solids: Principles, Methodology and Applications: Second Edition*. 2013.

[65] C. R. Brundle, C. A. Evans, and S. Wilson, *Encyclopedia of materials characterization : surfaces, interfaces, thin films*. 1992.

[66] S. Chakraborty, A. K. Kole, and P. Kumbhakar, “Room temperature chemical

synthesis of flower-like ZnO nanostructures," *Mater. Lett.*, vol. 67, no. 1, pp. 362–364, 2012.

[67] J. Majeed, J. Ramkumar, S. Chandramouleeswaran, and A. K. Tyagi, "Effect of Synthesis Protocol on the Surface Charge of Zinc Oxide Nanoparticles and its Consequence on Sorption Ability," *Sep. Sci. Technol.*, vol. 50, no. 3, pp. 404–410, 2015.

[68] K. J. Hartlieb, C. L. Raston, and M. Saunders, "Controlled scalable synthesis of ZnO nanoparticles," *Chem. Mater.*, vol. 19, no. 23, pp. 5453–5459, 2007.

[69] Y. Han *et al.*, "Aggregation and dissolution of ZnO nanoparticles synthesized by different methods: Influence of ionic strength and humic acid," *Colloids Surfaces A Physicochem. Eng. Asp.*, vol. 451, no. 1, pp. 7–15, 2014.

[70] M. Elango, S. Ranjith, C. Balakumar, K. M. P. Nazeer, S. Vairam, and M. Thamilselvan, "Synthesis, structural, optical and thermal analysis of nanostructured ZnO," *Int. J. Mater. Res.*, vol. 104, no. 3, pp. 308–313, 2013.

[71] Shamsuzzaman, A. Mashrai, H. Khanam, and R. N. Aljawfi, "Biological synthesis of ZnO nanoparticles using C. albicans and studying their catalytic performance in the synthesis of steroidal pyrazolines," *Arab. J. Chem.*, vol. 10, no. August 2014, pp. 1530–1536, 2013.

[72] N. Shanmugam, K. Dhanaraj, G. Viruthagiri, K. Balamurugan, and K. Deivam, "Synthesis and characterization of surfactant assisted Mn2+ doped ZnO nanocrystals," *Arab. J. Chem.*, vol. 9, pp. S758–S764, 2016.

[73] M. I. Khalil, M. M. Al-Qunaibit, A. M. Al-zahem, and J. P. Labis, "Synthesis and characterization of ZnO nanoparticles by thermal decomposition of a curcumin zinc complex," *Arab. J. Chem.*, vol. 7, no. 6, pp. 1178–1184, 2014.

[74] Y. T. Prabhu, K. V. Rao, V. S. S. Kumar, and B. S. Kumari, "Synthesis of ZnO Nanoparticles by a Novel Surfactant Assisted Amine Combustion Method," *Adv. Nanoparticles*, vol. 2, no. 1, pp. 45–50, 2013.

[75] G. Konig *et al.*, "Mechanical properties of completely autologous human tissue engineered blood vessels compared to human saphenous vein and mammary artery," *Biomaterials*, vol. 30, no. 8, pp. 1542–1550, 2009.

[76] M. R. Williamson, R. Black, and C. Kielty, "PCL-PU composite vascular scaffold production for vascular tissue engineering: Attachment, proliferation and bioactivity of human vascular endothelial cells," *Biomaterials*, vol. 27, no. 19, pp. 3608–3616, 2006.

[77] X. Y. Ma and W. D. Zhang, "Effects of flower-like ZnO nanowhiskers on the

mechanical, thermal and antibacterial properties of waterborne polyurethane," *Polym. Degrad. Stab.*, vol. 94, no. 7, pp. 1103–1109, 2009.

[78] A. A. Neyfakh, C. M. Borsch, and G. W. Kaatz, "Fluoroquinolone resistance protein NorA of Staphylococcus aureus is a multidrug efflux transporter," *Antimicrobial Agents and Chemotherapy*, vol. 37, no. 1. pp. 128–129, 1993.

[79] R. Brayner, R. Ferrari-Iliou, N. Brivois, S. Djediat, M. F. Benedetti, and F. Fiévet, "Toxicological impact studies based on Escherichia coli bacteria in ultrafine ZnO nanoparticles colloidal medium," *Nano Lett.*, vol. 6, no. 4, pp. 866–870, 2006.

[80] L. H. Peterson, R. E. Jensen, and J. Parnell, "Mechanical Properties of Arteries in Vivo," *Circ. Res.*, vol. 8, no. 3, pp. 622–639, 1960.

Annex

.

Bacterial Viability Assay

The experimental procedure for the determination of the bacterial viability was carried out in the course of 3 days and involves the following steps:

Day 1:

The TSB (Trypstic soy broth) and PCA (Plate count Agar) medium were prepared according to the manufacturer's instructions. Both mediums were sterilized using an autoclave.

The petri dishes (90 mm) were prepared with PCA culture medium. The plates were stored at 4ºC. the entire process was conducted under aseptic conditions in a laminar flow chamber and in the vicinity of a flame, so as to avoid contamination of the culture medium by microorganisms.

The culture of E.coli was incubated in TSB at 37ºC under constant agitation (180 rmp) over night (16h)

Day 2:

The optical density of the bacterial culture, prepared the precious day, was read on a spectrophotometer with a 600 nm wavelength. A sample of TSB was used as blank.

2 ml of bacterial culture were were washed by centrifugation, with replacement of the supernatant by phosphate buffer (pH=7.2). This procedure was repeated twice to ensure the removal of traces of culture medium.

After that, the culture was resuspended in buffer using a volume which guarantees a concentration of bacteria of $2.4x10^9$ cell/ ml. The volume of phosphate buffer used was determined based on the optical density measurements taken at the beginning of the procedure, assuming that one unity of optical density corresponds to a bacterial concentration of $8x10^8$ cell/ ml.

Meanwhile, 900 µl of buffer solution were placed inside microtubes alongside the membrane samples (disks with 12mm diameter), 2 ml microtubes were used to ensure that the membranes were not immobilized, guarantying a dynamic assay. 100 µL of the bacterial suspension were then added to each microtube. A microtube containing a known bacterial concentration ($2.4x10^8$ cell/mL) served as a control sample.

Each of this microtubes were incubated under constant stirring for one hour at room temperature, after which decimal dilutions of each sample were made. For each decimal dilutions (designated -1, -2, -3, -4, -5) a microtube was prepared with 900 µL of the buffer solution and 100 µL of the incubated solution.

Finally, the culture plates were seeded, this consist of adding 100 µL of each decimal dilution to each plate. This was made in triplicate to calculate the mean and standard deviation. The inoculated plates were incubated overnight (16h) at a temperature of 37ºC (optimum temperature for E. coli growth).

Day 3:

The number of CFUs (Colony Forming Units) was counted on each plate. Counts performed on plates inoculated with the composite membrane and the pure PU membrane are compared with the count of the CFUs present in the controlled sample, thus allowing the determination of the reduction of bacterial viability, based on the following equation:

$$R = 100 - \frac{CFU_p \times 100}{CFU_c}$$

Where CFUp is the number of weighted Colony Forming Units in CFU/ mL, calculated as:

$$CFU_p = CFU \times V \times F_D$$

Where CFU is the count of the Colony Forming Units if an inoculated petri dish, V is the volume of the test suspension seeded on the plate (0.1 mL) and F_D is the dilution factor.

The table below shows the results used in Fig. 29 and Fig. 30.

Table 13: Table with the CFU from the E.coli test

Sample	Dilution	CFI	Volume (ml)	Dilution Factor	Weighted CFU (CFU/ ml)	Reduction (%)
C	-4	209	0.1	1.00E+04	2.09E+05	1.73E+05
	-4	175	0.1	1.00E+04	1.75E+05	
	-4	135	0.1	1.00E+04	1.35E+05	
0%	-4	134	0.1	1.00E+04	1.34E+05	22.5433526
	-4	38	0.1	1.00E+04	3.80E+04	38.03468208
	-4	92	0.1	1.00E+04	9.20E+04	46.82080925
10%	-4	66	0.1	1.00E+04	6.60E+04	61.84971098
	-4	89	0.1	1.00E+04	8.90E+04	48.55491329
	-4	103	0.1	1.00E+04	1.03E+05	40.46242775
25%	-4	85	0.1	1.00E+04	8.50E+04	50.86705202
	-4	71	0.1	1.00E+04	7.10E+04	58.95953757
	-4	73	0.1	1.00E+04	7.30E+04	57.80346821
50%	-4	68	0.1	1.00E+04	6.80E+04	60.69364162
	-4	53	0.1	1.00E+04	5.30E+04	69.36416185
	-4	51	0.1	1.00E+04	5.10E+04	70.52023121

Table 14: Table with the CFU from the S.aureus test

Sample	Dilution	CFI	Volume (ml)	Dilution Factor	Weighted CFU (CFU/ ml)	Reduction (%)
C	-5	213	0.1	100000	2130000	2083333.333
	-5	183	0.1	100000	1830000	
	-5	229	0.1	100000	2290000	
0	-4	162	0.1	10000	162000	92.22399876
	-4	192	0.1	10000	192000	90.78399853
	-4	209	0.1	10000	209000	89.96799839
10%	-4	84	0.1	10000	84000	95.96799935
	-4	69	0.1	10000	69000	96.68799947
	-4	63	0.1	10000	63000	96.97599952
25%	-4	42	0.1	10000	42000	97.98399968
	-4	71	0.1	10000	71000	96.59199945
	-4	62	0.1	10000	62000	97.02399952
50%	-4	85	0.1	10000	85000	95.91999935
	-4	61	0.1	10000	61000	97.07199953
	-4	73	0.1	10000	73000	96.49599944